Physics – Uspekhi **61** (1) 29 – 51 (2018)

INSTRUMENTS AND METHODS OF INVESTIGATION PACS numbers: 29.20.db, 29.20.dk, 29.27.Ac, 29.27.Bd, 29.27.Eg

Low emittance electron storage rings

E B Levichev

DOI: https://doi.org/10.3367/UFNe.2016.12.038014

Contents

Abstract. Low-emittance electron (positron) beams are essential for synchrotron light sources, linear collider damping rings, and circular Crab Waist colliders. In this review, the principles and methods of emittance minimization are discussed, prospects for developing relativistic electron storage rings with small beam phase volume are assessed, and problems related to emittance minimization are examined together with their possible solutions. The special features and engineering implementation aspects of various facilities are briefly reviewed.

Keywords: electron storage ring, emittance, brightness, synchrotron light source

1. Introduction

The transverse phase volume (emittance) of a beam in an electron storage ring is an important parameter that often determines the setup operation efficiency. Very low emittance is essential for damping rings, which prepare dense electron and positron beams with extremely small dimensions in order to obtain large luminosity in linear colliders [1]. Small emittance is also important for circular e^+e^- colliders with a Crab Waist collision scheme, in which bunches with very small vertical size can intersect at a quite large angle [2]. The new collision scheme results in luminosity enhancement by one to two orders of magnitude with respect to traditional head-on collision schemes. However, the highest demand for ideas and approaches regarding emittance reduction is provided by synchrotron radiation (SR) sources, because their main parameter — brightness — is determined by the emittance [3].

Currently, there are over 40 operating storage rings around the world used as SR sources, in which scientists perform various kinds of research in the fields of physics, chemistry, biology, medicine, geology, archaeology, and material sciences. The SR from these sources is also used for technological applications. This is the most popular type of electron storage ring with ultrarelativistic energies ($E > 1$ GeV).

There are several generations of SR sources, and the emittance becomes smaller with every new generation. First-generation storage rings had the horizontal emittance $\varepsilon_x \sim 300-500$ nm (emittance is measured in [m rad] units, but for simplicity we omit the radian angular unit here and hereafter) and were initially designed for particle physics experiments. Second-generation storage rings were specialized facilities with the emittance $\varepsilon_x \sim 20$–100 nm, used for experiments with SR. Third-generation devices are now the most popular and advanced ones, having the emittance $\varepsilon_x \sim 1-10$ nm and generating high-brightness X-ray beams.

Until recently, it was believed that the development of X-ray radiation sources based on electron storage rings

E B Levichev Budker Institute of Nuclear Physics,
Siberian Branch of the Russian Academy of Sciences,
prosp. Akademika Lavrent'eva 13/3, 630090 Novosibirsk,
Russian Federation
E-mail: levichev@inp.nsk.su

Received 15 November 2016
Uspekhi Fizicheskikh Nauk **188** (1) 31 – 54 (2018)
DOI: https://doi.org/10.3367/UFNr.2016.12.038014
Translated by A L Chekhov; edited by A M Semikhatov

had reached its limit, and the fourth-generation term was assigned to free electron lasers based on linear accelerators [4] or multi-pass accelerator recuperators [5]. However, in 2014, National Synchrotron Light Source II (NSLS II) started operation at Brookhaven National Laboratory with the electron beam energy $E = 3$ GeV, an orbit length of 792 m, and $\varepsilon_x \approx 0.5$ nm [6]. In 2016, the MAX IV storage ring was launched at the MAX IV laboratory at Lund University (Sweden) with $E = 3$ GeV, a perimeter of 528 m, and the emittance $\varepsilon_x \approx 0.2-0.3$ nm [7]. An upgrade of the European Synchrotron Radiation Facility (ESRF) has been started in France (Grenoble) [8]. In fact, this will be a new storage ring based on the existing infrastructure. This new device will have the same energy and orbit length (6 GeV and 844 m), but its emittance will be decreased by a factor of 30, to $\varepsilon_x \approx 0.13$ nm. Following Winick, who wrote in [9] that every new generation of radiation source improves one of the important parameters (brightness, coherence, etc.) by approximately one order of magnitude, we can assert the emergence of the new fourth generation of circular SR sources.

Many laboratories in Europe, the USA, Japan, and China have plans to create new (or upgrade existing) SR sources with the horizontal emittance much lower than 1 nm. There are discussions of the possibility of obtaining $\varepsilon_x \sim 5-10$ pm, which is comparable with the diffraction size of the radiation source with $\lambda \sim 1$ Å (see, e.g., [10]).

We note that such an impressive decrease in the phase volume occurred not due to new ideas but due to gradual and constant progress in physics and the technology of circular accelerators of charged particles: the appearance of effective simulation algorithms for beam motion and a magnetic field, the design of lenses with shorter focal lengths, increase in the beam parameter measurement accuracy, the development of new vacuum technologies, etc.

In Russia, experiments on synchrotron radiation are performed at the National Research Center 'Kurchatov Institute' (NRC KI) using the second-generation Kurchatov Synchrotron Radiation Source (KSRS), which is based on the Siberia-2 storage ring with an energy of 2.5 GeV and the emittance $\varepsilon_x \approx 90$ nm [11], and at the Budker Institute of Nuclear Physics (BINP) SB RAS using two storage rings, VEPP-3 and VEPP-4M,[1] which are mainly used for experiments in the field of elementary particle physics (first generation) [12].

2. Relativistic electron beam emittance

In a circular accelerator with an equilibrium orbit located in the horizontal (median) plane, the transverse motion of an ultra-relativistic electron is described by equations for betatron oscillations,

$$\frac{\mathrm{d}^2 x}{\mathrm{d}s^2} + K_x(s)\, x = \frac{1}{\rho(s)}\,\frac{\Delta E}{E_0}\,, \tag{1}$$

$$\frac{\mathrm{d}^2 y}{\mathrm{d}s^2} + K_y(s)\, y = 0\,, \tag{2}$$

where x and y are horizontal and vertical deviations of the particle from the equilibrium orbit and the independent variable s corresponds to the coordinate along the orbit. Periodic functions $K_x(s)$ and $K_y(s)$ are coefficients in Eqns (1) and (2), and they depend on the vertical magnetic field at the orbit $B_y(s)$ and on its gradient $G(s) = \partial B_y/\partial x$:

$$K_x(s) = \left(\frac{B_y(s)}{B\rho}\right)^2 + \frac{G(s)}{B\rho}\,, \quad K_y = -\frac{G(s)}{B\rho}\,,$$

where the magnetic rigidity $B\rho$ is related to the total momentum p_0 (the total energy E_0) of an equilibrium electron as $B\rho = p_0/e \approx E_0/ce$. The existence of the right-hand side in (1) is explained by the fact that for a particle with a nonequilibrium energy, the curvature radius $\rho(s)$ in the field B_y and hence the particle motion trajectory are different from those in the case of the equilibrium energy E_0. It is assumed that there is no coupling between betatron oscillations (its influence is discussed in Section 5.2).

Solving Eqn (2) gives vertical betatron oscillations in the form (Floquet solution)

$$y(s) = \sqrt{2J_y\beta_y(s)}\,\cos\left(\phi_y(s) + \phi_{0y}\right), \tag{3}$$

where constants J_y and ϕ_{0y} are defined by the initial conditions, and the betatron functions (the amplitude $\beta_y(s)$ and the phase $\phi_y(s)$) are related as

$$\phi_y(s) = \int_{s_0}^{s} \frac{\mathrm{d}s}{\beta_y(s)}\,. \tag{4}$$

Expression (3) describes pseudoharmonic oscillations with the instantaneous amplitude $A_y(s) = (2J_y\beta_y(s))^{1/2}$ and instantaneous wavelength $\lambda_y(s) = 2\pi\beta_y(s)$, where the betatron function is a periodic solution of the equation $2\beta_y\beta_y'' - \beta_y'^2 + 4\beta_y^2 K_y = 4$.

The integral in (4), taken along the orbit, is independent of the integration limits and determines the betatron oscillation frequency (in units of the circulation frequency)

$$\nu_y = \frac{1}{2\pi}\oint \frac{\mathrm{d}s}{\beta_y(s)}\,. \tag{5}$$

It is obvious that the higher the focusing is, the higher the betatron frequency.

Direct integration over the phase volume

$$\oint y'\,\mathrm{d}y = \oint y'\,\frac{\mathrm{d}y}{\mathrm{d}s}\,\mathrm{d}s = \oint y'^2\,\mathrm{d}s = J_y$$

shows that the constant of motion J_y is an action integral, which is conserved in a conservative system.

The solution of (1) is different from (3) due to the nonzero right-hand term. We express the horizontal displacement of a particle as a sum of betatron and 'energetic' motion,

$$x(s) = x_\beta(s) + x_E(s) = x_\beta(s) + \eta(s)\,\frac{\Delta E}{E_0}\,, \tag{6}$$

where we introduce a dispersion function $\eta(s)$. Now, substituting (6) in (1), we obtain two equations: one for the horizontal betatron motion (index β is omitted for x),

$$\frac{\mathrm{d}^2 x}{\mathrm{d}s^2} + K_x(s)\, x = 0 \tag{7}$$

and the other

$$\frac{\mathrm{d}^2 \eta}{\mathrm{d}s^2} + K_x(s)\,\eta = \frac{1}{\rho(s)}\,, \tag{8}$$

[1] VEPP: from the Russian abbreviation for *Colliding Electron–Positron Beams*.

with a periodic solution defining the dispersion function. Expression (6) shows that a particle with a nonequilibrium energy experiences betatron oscillations $x_\beta(s)$ around a new dispersion orbit $x_E(s)$. Horizontal betatron oscillations have the same form as the vertical ones in Eqn (3),

$$x(s) = \sqrt{2J_x\beta_x(s)}\cos\phi_x\,, \tag{9}$$

$$x'(s) = -\sqrt{\frac{2J_x}{\beta_x(s)}}\,(\sin\phi_x + \alpha_x(s)\cos\phi_x)\,, \tag{10}$$

where the initial phase is set to zero (which can be done due to the periodicity condition) and the parameter $\alpha(s) = -\beta'(s)/2$ is introduced. The prime stands for the derivative over s.

The constant, which is an integral of motion, can be expressed as the Courant–Snyder invariant [13]

$$2J_x = \gamma_x(s)\,x^2 + 2\alpha_x(s)\,xx' + \beta_x(s)\,x'^2\,, \tag{11}$$

where another parameter is introduced:

$$\gamma(s) = \frac{1+\alpha^2(s)}{\beta(s)}\,. \tag{12}$$

Expression (11) defines the phase trajectory of particles in the (x, x') coordinates, which is easily seen to be an ellipse (Fig. 1). The tilt of the ellipse axes varies during the particle motion, but its area $S = 2\pi J_x$ is conserved.

For an ensemble of particles with different initial conditions (that is, with different values of the action J), the averaging of second moments of the beam distribution function using (9) and (10) gives

$$\langle x^2\rangle = \beta_x\langle J_x\rangle\,,\quad \langle x'^2\rangle = \gamma_x\langle J_x\rangle\,,\quad \langle xx'\rangle = -\alpha_x\langle J_x\rangle\,. \tag{13}$$

The root mean square emittance of the beam is the square root of the second moment matrix determinant

$$\varepsilon_x = \sqrt{\langle x^2\rangle\langle x'^2\rangle - \langle xx'\rangle^2} = \langle J_x\rangle\,,$$

where expression (12) is taken into account. This means that the beam emittance is equal to an integral of motion averaged over all particles of the distribution. The above considerations are also valid for the vertical motion.

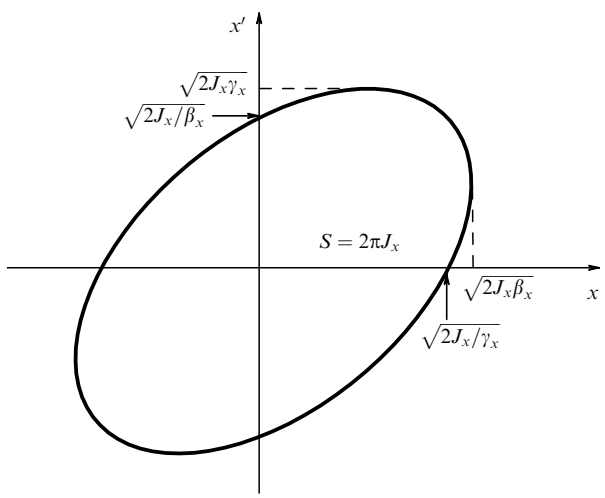

Figure 1. Phase ellipse defined by (11) with the area $S = 2\pi J_x$.

2.1 Betatron oscillation damping due to synchrotron radiation

According to the Liouville theorem, for motion described by Hamilton equations, an integral of action and, in particular, the emittance are conserved. But a relativistic electron, while rotating in a magnetic field, experiences acceleration and emits energy. Precisely synchrotron radiation determines the equilibrium emittance in high-energy electron storage rings.

SR is emitted into a narrow cone with a characteristic angle $\sim 1/\gamma$, $\gamma \gg 1$, directed along the tangent to the instantaneous trajectory of the particle. The radiation power of a particle with an energy E moving along a circular orbit with radius ρ in a transverse magnetic field B has the form [14]

$$P_\gamma = \frac{cC_\gamma}{2\pi}\,\frac{E^4}{\rho^2} = \frac{e^2c^3C_\gamma}{2\pi}\,E^2B^2\,, \tag{14}$$

where

$$C_\gamma = \frac{e^2}{3\varepsilon_0(m_0c^2)^4} \approx 8.846\times10^{-5}\ \text{m GeV}^{-3}\,.$$

If nothing is done, the beam energy would decrease due to SR, and dispersive orbit (6) would change continuously until the beam is destroyed on the vacuum chamber wall. Therefore, there are special devices in the storage rings, accelerating resonators, which create a longitudinal radio-frequency (RF) electric field in the equilibrium orbit. This field is phase-synchronized to the moment of beam flight in such a way that the average SR energy loss is compensated. However, the resonator field restores only the longitudinal momentum of the particle, while its transverse component diminishes. This leads to betatron oscillation damping and hence to a decrease in the beam emittance. The appearance of such a radiation reaction force can be easily illustrated for vertical betatron motion (Fig. 2).

We assume that the photon is emitted along the direction of electron instantaneous motion (the influence of the nonzero radiation cone angle $\sim 1/\gamma$ is discussed in Section 2.2), and it results in a change in the total momentum p by a value δp. After the emission, neither the particle coordinate nor the trajectory tangent y_0' change compared to the equilibrium orbit. However, after the flight through the resonator, the longitudinal momentum of the particle is restored and the trajectory slope changes:

$$y_1 = y_0\,,$$

$$y_1' = \frac{p_y}{p+\delta p} \approx \frac{p_y}{p}\left(1-\frac{\delta p}{p}\right) = y_0'\left(1-\frac{\delta p}{p}\right) < y_0'\,. \tag{15}$$

Substituting (15) in (11), we obtain a variation of the motion integral [15]

$$\mathrm{d}J_y = -(\alpha_y y_0 y_0' + \beta_y y_0'^2)\,\frac{\delta p}{p}\,.$$

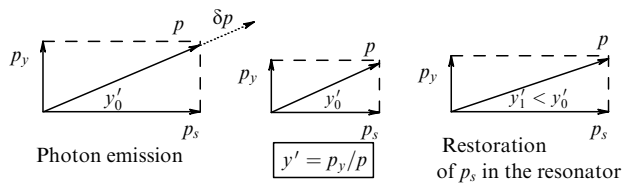

Figure 2. Decrease in the particle vertical momentum p_y due to SR.

Averaging the last expression over the beam and using (13), we obtain

$$\mathrm{d}\varepsilon_y = \langle \mathrm{d}J_y \rangle = -\varepsilon_y(-\alpha_y^2 + \beta_y\gamma_y)\,\frac{\delta p}{p} = -\varepsilon_y\,\frac{\delta p}{p}\,.$$

Because the radiation energy loss U_0 during one revolution is small with respect to the total energy of the beam $E_0 \approx p_0 c$ (usually, $U_0 \sim 10^{-3}E_0$), the particle momentum variation is slow, and the momentum can be averaged over the period T_0, whence we have the following equation for the vertical emittance:

$$\frac{\mathrm{d}\varepsilon_y}{\mathrm{d}t} = -\frac{\varepsilon_y}{T_0}\oint\frac{\mathrm{d}p}{p_0} \approx -\frac{U_0}{E_0 T_0}\,\varepsilon_0 = -\frac{2}{\tau_y}\,\varepsilon_y\,, \tag{16}$$

with the solution

$$\varepsilon_y(t) = \varepsilon_y(0)\exp\left(-2\,\frac{t}{\tau_y}\right), \tag{17}$$

where the damping time

$$\tau_y = 2\,\frac{E_0}{U_0}\,T_0 \tag{18}$$

is related to the oscillation amplitude. Expressions (16) and (17) describing phase volume damping contain an additional factor of 2 because $\varepsilon_y \sim A_y^2$ according to (3).

We now express the average radiative energy loss U_0 due to SR in terms of the storage ring parameters. From expression (14) for the radiation power, we have

$$U_0 = \oint P_\gamma\,\mathrm{d}t \approx \oint P_\gamma\,\frac{\mathrm{d}s}{c} = \frac{C_\gamma}{2\pi}\,E_0^4\oint\frac{\mathrm{d}s}{\rho^2} = \frac{C_\gamma}{2\pi}\,E_0^4 I_2\,, \tag{19}$$

where we introduce a notation for the second radiation integral [16]

$$I_2 = \oint\frac{\mathrm{d}s}{\rho^2}\,. \tag{20}$$

We see that the betatron oscillation damping time (18) depends on the cube of the beam energy and on the curvature radius of the beam trajectory in the magnetic field: the smaller the radius (the larger the magnetic field), the faster the vertical emittance diminishes.

The damping mechanism is the same for horizontal betatron oscillations. However, according to (6), the emission of a photon with an energy ΔE_γ results in a change $x_E(s) = \eta(s)\,\Delta E_\gamma/E_0$ in the closed orbit about which the betatron oscillations take place. This makes the calculations more complicated and we only show the result without the derivation, which can be found in circular accelerator textbooks (see, e.g., [17]):

$$\varepsilon_x(t) = \varepsilon_x(0)\exp\left(-2\,\frac{t}{\tau_x}\right), \quad \tau_x = \frac{2}{J_x}\,\frac{E_0}{U_0}\,T_0\,, \tag{21}$$

where the dimensionless decrement

$$J_x = 1 - \frac{I_4}{I_2} \tag{22}$$

takes the influence on the damping of the specific magnet lattice into account in terms of the radiation integrals I_2 and

$$I_4 = \oint\frac{\eta}{\rho}\left(\frac{1}{\rho^2} + 2\,\frac{G}{B\rho}\right)\mathrm{d}s\,. \tag{23}$$

Although we consider the transverse emittance here, we note for completeness that SR also leads to the damping of longitudinal synchrotron oscillations. If the reduced electron energy is different from the equilibrium one by $\delta(t) = \Delta E/E_0$ and its longitudinal coordinate with respect to the beam center is $z(t)$, the longitudinal ('energy') emittance can be defined similarly to the transverse one:

$$\varepsilon_E = \sqrt{\langle\delta^2\rangle\langle z^2\rangle - \langle\delta z\rangle^2}\,.$$

Under the action of SR, the longitudinal emittance decreases as

$$\varepsilon_E(t) = \varepsilon_E(0)\exp\left(-2\,\frac{t}{\tau_E}\right), \quad \tau_E = \frac{2}{J_E}\,\frac{E_0}{U_0}\,T_0\,, \tag{24}$$

where

$$J_E = 2 + \frac{I_4}{I_2}\,.$$

It is easy to see that $J_x + J_E = 3$. For a planar orbit without the coupling of vertical motion with longitudinal and horizontal ones, $J_y = 1$. Generally, this is not the case, but a detailed analysis of damping of all three oscillation modes shows that the Robinson theorem holds [18]:

$$J_x + J_y + J_E = 4\,. \tag{25}$$

According to (25), the damping enhancement of any oscillation mode is accompanied by a damping reduction in another mode.

2.2 Quantum effects of radiation. Equilibrium emittance

In the foregoing, we used a classical model of radiation (the equations did not contain the Planck constant) and assumed that the energy can be emitted in arbitrarily small portions. These considerations led us to the result in (17) and (18), which corresponds to a beam size reduction to zero.

In reality, the energy is emitted almost instantaneously, randomly, and statistically independently by single photons with $\Delta E_\gamma = \hbar\omega$. Because the photon energy is much less than the electron energy, the weak 'kicks' that accompany every emission event lead to particle velocity diffusion. Although the quantum emission changes neither the coordinate x_0 nor the trajectory angle x_0', the orbit along which these quantities are measured changes abruptly (Fig. 3) and, according to (6), the new coordinate and angular deviation can be expressed as

$$x_\beta = x_0 + \eta(s)\,\frac{\Delta E_\gamma}{E_0}\,, \quad x_\beta' = x_0' + \eta'(s)\,\frac{\Delta E_\gamma}{E_0}\,.$$

Substituting these expressions in (11) and averaging over the betatron oscillation phase and the distribution of particles in the beam, we obtain the increase in the horizontal emittance after one emission event:

$$\Delta\varepsilon_x = \frac{1}{2}\,\frac{\langle\Delta E_\gamma^2\rangle}{E_0^2}\,H(s)\,, \tag{26}$$

$$H(s) = \gamma_x(s)\,\eta^2(s) + 2\alpha_x(s)\,\eta(s)\,\eta'(s) + \beta_x(s)\,\eta'^2(s)\,. \tag{27}$$

The function $H(s)$ is often called the Courant–Snyder dispersion invariant, although, strictly speaking, it is constant only in the regions where the magnetic field is zero.

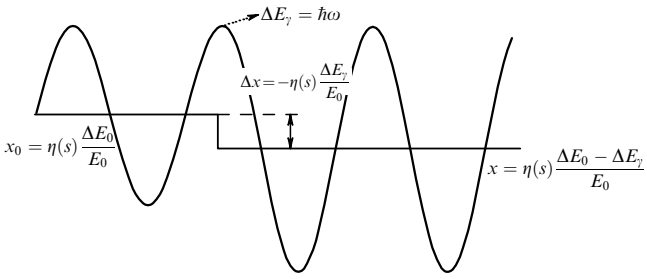

Figure 3. Betatron oscillation amplitude change due to the quantum character of emission.

If we multiply (26) by the average number of photons $\dot{N}$ emitted per unit of orbit length and integrate along the storage ring perimeter Π, then the obtained value characterizes the average rate of emittance growth due to fluctuations. Accounting for betatron oscillation damping (21) leads to the equation

$$\frac{\mathrm{d}\varepsilon_x}{\mathrm{d}t} = \frac{1}{2E_0^2\Pi}\oint \dot{N}\langle\Delta E_\gamma^2\rangle\, H(s)\,\mathrm{d}s - \frac{2}{\tau_x}\,\varepsilon_x\,.$$

The theory of SR provides the product of photon emission frequency and photon root-mean-square energy in the form

$$\dot{N}\langle\Delta E_\gamma^2\rangle = 2C_\mathrm{q}\gamma^2 E_0\,\frac{P_\gamma}{\rho}\,,$$

$$C_\mathrm{q} = \frac{55}{32\sqrt{3}}\,\frac{\hbar}{mc} \approx 3.832\times 10^{-13}\ \mathrm{m}\,. \tag{28}$$

Using this expression together with (14), we obtain

$$\frac{\mathrm{d}\varepsilon_x}{\mathrm{d}t} = C_\mathrm{q}\gamma^2\,\frac{2}{J_x\tau_x}\,\frac{I_5}{I_2} - \frac{2}{\tau_x}\,\varepsilon_x\,,$$

where we introduce the fifth radiation integral

$$I_5 = \oint \frac{H(s)}{|\rho^3(s)|}\,\mathrm{d}s\,. \tag{29}$$

Balancing the quantum induced oscillations and 'classical' damping of betatron oscillations, defined by the condition $\mathrm{d}\varepsilon_x/\mathrm{d}t = 0$, leads to the equilibrium emittance

$$\varepsilon_x = C_\mathrm{q}\gamma^2\,\frac{I_5}{J_x I_2}\,. \tag{30}$$

The equilibrium emittance depends on the electron energy (quadratically), on the optical functions of the storage ring (via the $H(s)$ function), and on the radii of the bending magnets. Generally, expression (30) holds for small currents (the emittance increases for high currents), and it does not take the possible coupling of transverse oscillations into account.

For a planar orbit without coupling of transverse degrees of freedom, the vertical function vanishes, $H_y(s) = 0$, and the quantum induced mechanism described above is absent. Reducing the vertical emittance to zero is limited by the finite angle of emission quanta $\sim 1/\gamma$, which leads to the equilibrium value

$$\varepsilon_{y\,\mathrm{min}} = \frac{13}{55}\,\frac{C_\mathrm{q}}{J_y}\,\frac{\oint \mathrm{d}s\,\beta_y(s)/|\rho^3|}{\oint \mathrm{d}s\,1/\rho^2}\,, \tag{31}$$

which is very small (approximately $1/\gamma^2$ times the equilibrium horizontal emittance). For a real storage ring, the vertical emittance is determined by the coupling of transverse oscillations, by the vertical orbit distortion, which leads to the appearance of $H_y(s) \neq 0$ (characteristic values $\varepsilon_y = (10^{-3}-10^{-2})\,\varepsilon_x$), by the scattering of particles on each other inside the bunch, and by other effects.

The simultaneous action of the quantum 'noise' and damping (24) also determines the equilibrium longitudinal emittance. The steady-state relative root-mean-square dispersion of the particle energies σ_δ in the beam can be found using the relation

$$\sigma_\delta^2 = C_\mathrm{q}\gamma^2\,\frac{I_3}{J_E I_2}\,,\quad I_3 = \oint \frac{\mathrm{d}s}{|\rho^3|}\,, \tag{32}$$

and the longitudinal size of the bunch

$$\sigma_z = \frac{\alpha c}{\omega_\mathrm{s}}\,\sigma_\delta\,, \tag{33}$$

where ω_s is the frequency of small synchrotron oscillations and the factor α, which characterizes the change in the orbit length for a particle with a nonequilibrium energy,

$$\frac{\Delta\Pi}{\Pi} = \delta\alpha\,,$$

is defined using the first radiation integral:

$$\alpha = \frac{I_1}{\Pi} = \frac{1}{\Pi}\oint \frac{\eta(s)}{\rho}\,\mathrm{d}s\,. \tag{34}$$

We note that the energy spread in the beam, Eqn (32), depends solely on the storage ring energy and the curvature radius of the equilibrium orbit and does not depend on the parameters of the accelerating system. At the same time, the longitudinal size of the beam, Eqn (33), depends on the synchrotron oscillation frequency and can be controlled by changing the parameters of the accelerating system (for example, the voltage on the resonator gap or the RF field oscillation frequency).

For all three degrees of freedom, the photons are emitted in small portions (with respect to the electron energy) with the emission events being random and statistically independent. Using the central limit theorem, it can be shown that the stable particle distribution over all coordinates is Gaussian. For example, in the case of the horizontal coordinate,

$$\Psi(x) = \frac{1}{\sqrt{2}\sigma_x}\exp\left(-\frac{x^2}{2\sigma_x^2}\right),$$

where $\sigma_x = \sqrt{\varepsilon_x\beta_x}$ is the root-mean-square size of the beam. We note, however, that the radiation source size is not necessarily equal to the betatron size. If the radiation is emitted from the azimuth s with the dispersion function $\eta(s) \neq 0$, then, due to energy diffusion, the effective root-mean-square size of the source is expressed as

$$\sigma_{x\,\mathrm{eff}} = \sqrt{\varepsilon_x\beta_x + \left(\frac{\eta(s)\,\Delta E}{E_0}\right)^2}\,. \tag{35}$$

3. Lattice function optimization

To achieve low emittance for a given energy, we can, in accordance with (30), increase the damping (increase the

integral I_2), optimize the optical functions in the bending magnets (decrease I_5), or increase the decrement J_x in Eqn (22) by varying the integral I_4. All these methods are used, although the last one is limited by the condition $J_x + J_E = 3$. Increasing J_x decreases J_E, which can lead to the enhancement ('antidamping') of synchrotron oscillations. Even if the motion remains stable, this results in an increase in energy spread (32) and bunch length (33), which is often undesirable for experiments with a short time resolution.

We qualitatively analyze consequences of the emittance reduction problem. For an isomagnetic lattice (bending radius of the magnets $\rho(s) = \text{const}$), when the beating of the betatron functions is small, the dispersion function can be approximated as [19]

$$\eta(s) \approx \left(\frac{\alpha R}{\nu_x}\,\beta_x(s)\right)^{1/2},$$

where R is the average radius of the storage ring ($\Pi = 2\pi R$), ν_x is the horizontal betatron oscillation frequency, and momentum compaction factor (33) in a smooth approximation is $\alpha \approx \nu_x^{-2}$. Substituting these expressions in (27), we obtain the following expression for equilibrium emittance (30):

$$\varepsilon_x = \frac{C_q \gamma^2}{J_x}\,\frac{R}{\rho \nu_x^3}\,. \tag{36}$$

To decrease the emittance, it is expedient to increase the magnet curvature radius, but this would lead to a larger storage ring size. The most efficient way is to increase the focusing and the betatron oscillation frequency ν_x. Vice versa, lattice function optimization for emittance reduction is often accompanied by stricter requirements for the focusing.

Expression (36), despite its simplicity, gives a rather good estimate for the equilibrium emittance, even for modern storage rings with a large beating of the betatron functions. For example, in the case of the Sibir-2 SR source at the Kurchatov Institute [11] with the beam energy 2.5 GeV, $\nu_x = 7.7$, $R = 19.7$ m, $\rho = 4.9$ m, $R/\rho \approx 4$, and $J_x \approx 1$, estimate (35) gives the emittance 80 nm, while its exact value is around 90 nm.

3.1 Basic principles of magnet lattice optimization

In the late 1960s–early 1970s, in order to generate SR, scientists used synchrotrons and storage rings designed for particle physics. The first magnet lattice of an SR-dedicated storage ring was developed in 1975 by Chasman and Green [20]. Because the storage ring energy $E = 1.5$ GeV was not large, it was suggested that hard radiation be obtained by installing several periodic alternating magnets (wigglers) with a strong magnetic field (up to 4 T). Such devices need straight sections with zero dispersion and small values of the betatron functions (see Section 4.3), and this problem was successfully solved in the Chasman–Green (CG) lattice.

The storage ring consisted of six identical cells (superperiods); each included two achromatic bends separated by quadrupole lens triplets and a straight section with a zero dispersion function (Fig. 4a). The achromatic bend was constructed using two bending magnets (divided into two parts in the original CG lattice) with a focusing lens between them. In order to obtain a small beam size and high radiation brightness, the betatron functions in the magnets had to be small. Although there was no special optimization of the horizontal emittance in the CG lattice, small values of the β_x and η functions in the magnets decreased the emittance by one order of magnitude compared with 'conventional' electron storage rings with the same energy.

If the CG lattice is modified such that each superperiod contains only one achromatic bend, the Double Bend Achromat (DBA), lattice is obtained, as shown in Fig. 4b. This simple, robust, and compact lattice (especially if lens doublets are used instead of triplets) became the basis of many second- and third-generation SR sources.

The first expression for the minimal emittance was obtained for the DBA lattice of the Sibir-2 SR source [21] created by the BINP SB RAS for the Kurchatov Institute. At approximately the same time, research on electron storage ring emittance optimization was performed in other laboratories around the world [22, 23].

For an isomagnetic lattice, $\rho(s) = \text{const}$ and equilibrium emittance (30) can be expressed as

$$\varepsilon_x = \frac{C_q \gamma^2}{J_x}\,\frac{\langle H(s)\rangle_m}{\rho}\,, \tag{37}$$

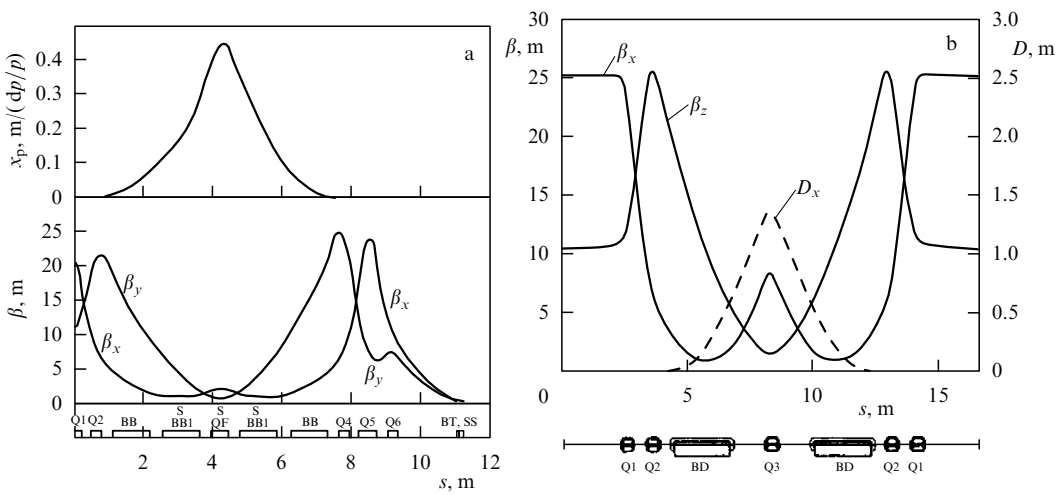

Figure 4. (a) The original CG superperiod. Upper curve: dispersion function, lower curves: betatron functions (adapted from [20]). (b) The DBA superperiod. The dispersion function D_x is shown with a dashed curve (scale to the right). Betatron functions are shown by solid curves (scale to the left).

where angular brackets denote the averaging of the dispersion invariant $H(s)$ over the ring magnets. On the edge of the magnet adjacent to the dispersionless section, $\eta = \eta' = 0$. Inside the magnet,

$$\eta(\theta) = \rho(1 - \cos\theta)\,, \quad \eta'(\theta) = \sin\theta\,, \tag{38}$$

where $\theta = s/\rho$ is the bending angle in the field of the magnet. We assume that the betatron function in the magnet has a minimum $\beta_{x\mathrm{m}}(\theta_\mathrm{m})$. Then, neglecting weak focusing in a uniform field, we obtain

$$\alpha_x(\theta) = \left(\frac{\beta_{x\mathrm{m}}}{\rho} - \frac{\rho}{\beta_{x\mathrm{m}}}\right) \sin(\theta - \theta_\mathrm{m}) \cos(\theta - \theta_\mathrm{m})\,,$$

$$\beta_x(\theta) = \beta_{x\mathrm{m}} \cos^2(\theta - \theta_\mathrm{m}) + \frac{\rho^2}{\beta_{x\mathrm{m}}} \sin^2(\theta - \theta_\mathrm{m})\,.$$

Substituting these expressions together with (38) in (37) and calculating

$$\langle H \rangle = \frac{1}{\theta_0} \int_0^{\theta_0} H(\theta)\,\mathrm{d}\theta\,,$$

where the full magnet bend angle is $\theta_0 = L_0/\rho$, we obtain

$$\langle H \rangle = A\left(\beta_{x\mathrm{m}} + \frac{\rho^2}{\beta_{x\mathrm{m}}}\right) + \left(\beta_{x\mathrm{m}} - \frac{\rho^2}{\beta_{x\mathrm{m}}}\right)\left[B\cos(2\theta_\mathrm{m}) + C\sin(2\theta_\mathrm{m})\right]\,, \tag{39}$$

where the functions A, B, and C are defined as

$$A = 1 - \frac{1}{\theta_0}\sin\theta_0\,, \quad B = \frac{1}{\theta_0}\left[\sin\theta_0 - \frac{1}{4}\sin(2\theta_0) - \frac{\theta_0}{2}\right]\,,$$

$$C = \frac{1}{\theta_0}\left[-\cos\theta_0 + \frac{1}{4}\cos(2\theta_0) + \frac{3}{4}\right]\,.$$

By finding the minimum (39) from the condition $\mathrm{d}\langle H \rangle/\mathrm{d}\theta_\mathrm{m} = \mathrm{d}\langle H \rangle/\mathrm{d}\beta_{x\mathrm{m}} = 0$ and expanding the obtained expressions in a series in $\theta_0 \ll 1$, we obtain

$$\theta_\mathrm{m} = \frac{3}{8}\,\theta_0\left(1 - \frac{1}{240}\,\theta_0^2 + \ldots\right)\,,$$

$$\beta_{x\mathrm{m}} = \rho\sqrt{\frac{3}{320}}\,\theta_0\left(1 + \frac{47}{6720}\,\theta_0^2 + \ldots\right)\,, \tag{40}$$

$$\langle H \rangle = \frac{\rho}{4\sqrt{15}}\,\theta_0^3\left(1 - \frac{11}{210}\,\theta_0^2 + \ldots\right)\,. \tag{41}$$

Disregarding the terms in parentheses, which are quadratic in θ_0, we obtain the minimal emittance of the DBA (or CG) lattice:

$$\varepsilon_\mathrm{DBA} \approx \frac{C_\mathrm{q}\gamma^2}{J_x}\,\frac{\theta_0^3}{4\sqrt{15}}\,, \tag{42}$$

which for $J_x = 1$ is

$$\varepsilon_\mathrm{DBA}[\mathrm{m}] \approx 9.5 \times 10^{-8}\,E^2\,[\mathrm{GeV}]\,\theta_0^3\,. \tag{43}$$

The expressions presented show that the emittance can be decreased by dividing the storage ring into a large number of superperiods that contain magnets with a small bending angle θ_0. However, this result also explains the complications of emittance reduction. The optimal betatron function according to (40) is

$$\beta_{x\mathrm{m}} \approx \rho\sqrt{\frac{3}{320}}\,\theta_0 \approx \frac{L_0}{10}\,,$$

where L_0 is the magnet length. The smaller L_0 is, the smaller the required minimal beta function and the stronger should the focusing be. This creates problems, both technological (quadrupole lenses with a large field gradient are needed) and dynamical (see Section 5).

3.2 Review of low-emittance lattices

Simple expression (42) stimulated research on other types of magnet cells for low-emittance storage rings. It turned out that for any of them, the minimal emittance can be expressed as

$$\varepsilon_{x\,\mathrm{min}} = F\,\frac{C_\mathrm{q}\gamma^2}{J_x}\,\theta_0^3\,, \tag{44}$$

where the factor F describes the cell features, for example, $F_\mathrm{DBA} = 1/(4\sqrt{15})$. The minimum value of F can be obtained if the achromaticity of the bend is not required. At the same time, horizontal betatron and dispersion functions must have a minimum at the center of the magnet:

$$\beta_{x\mathrm{m}} = \frac{L_0}{2\sqrt{15}}\,, \quad \eta_\mathrm{m} = \frac{\theta_0 L_0}{24}\,. \tag{45}$$

In this case, the minimum emittance can be expressed as

$$\varepsilon_\mathrm{TME} \approx \frac{C_\mathrm{q}\gamma^2}{J_x}\,\frac{\theta_0^3}{12\sqrt{15}}\,. \tag{46}$$

This lattice is called the Theoretical Minimum Emittance (TME) lattice, and $F_\mathrm{TME} = 1/12\sqrt{15} = F_\mathrm{DBA}/3$. Characteristic dependences of optical functions for a TME lattice consisting of a central magnet and two quadrupole lens doublets are shown in Fig. 5.

The disadvantage of the TME lattice is the nonzero dispersion function in the straight sections, which limits the application of wigglers and undulators, which are the main

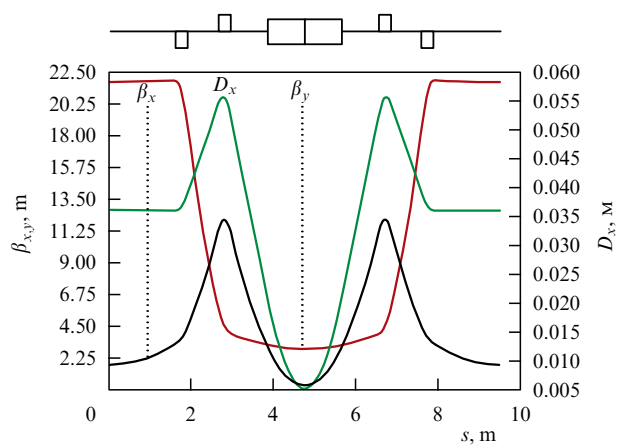

Figure 5. TME lattice that provides minimum emittance.

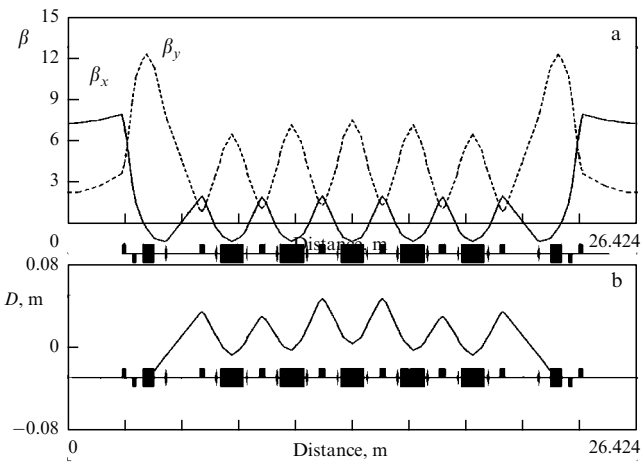

Figure 6. MBA lattice example: (a) betatron functions, (b) dispersion function.

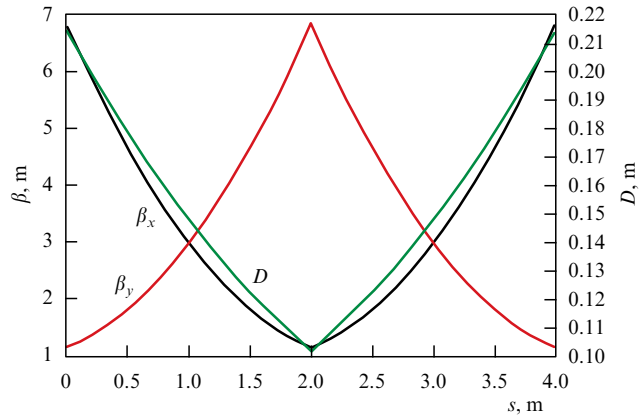

Figure 7. Optical functions of the FODO cell.

radiation sources in modern storage rings. Therefore, it is natural to combine low-emittance TME magnets with DBA magnets providing zero dispersion in straight sections. This combined lattice was named the MBA (Multiple Bend Achromat) lattice, with M referring to the total number of magnets in a superperiod.

As an example, in Fig. 6 we show a superperiod of the 7BA SR source MAX IV [24]. Its central part consists of five TME magnets. To the left and to the right of them two more magnets are placed in order to set the dispersion function to zero. The magnets are equipped with a vertical focusing, and it is therefore sufficient to place only one focusing lens between them, which makes the whole superperiod more compact.

It seems that the MBA minimum emittance should be the sum of the corresponding DBA (two magnets on the edges) and TME contributions. As an example, we consider a lattice with one central magnet (Triple Bend Achromat, TBA), for which the minimum emittance according to (42) and (46) is

$$\varepsilon_{\mathrm{TBA}} = \frac{2}{3}\,\varepsilon_{\mathrm{DBA}} + \frac{1}{3}\,\varepsilon_{\mathrm{TME}} = \frac{7}{9}\,\varepsilon_{\mathrm{DBA}}\,. \tag{47}$$

However, the matching of optical functions between the edge DBA magnet (length L_1 and radius ρ_1) and the central TME magnet (L_2 and ρ_2) leads to the condition [25]

$$\frac{L_2^3}{\rho_2^2} = 3\,\frac{L_1^3}{\rho_1^2}\,. \tag{48}$$

In the case of an isomagnetic lattice, $\rho_1 = \rho_2$ and Eqn (46) gives $L_2 = \sqrt[3]{3}L_1$. If we set $L_1 = L_2$, the condition $\rho_1 = \sqrt{3}\rho_2$ should be satisfied. It is possible to choose other values for the field and the length of central and edge magnets that satisfy condition (48) and which slightly change the TBA lattice minimum emittance [26]. For an isomagnetic lattice, the minimum emittance

$$\varepsilon_{\mathrm{TBA}} \approx \frac{C_q\gamma^2}{J_x}\,\frac{\theta_{\mathrm{TBA}}^3}{4\sqrt{15}} \tag{49}$$

has the same form as for the DBA lattice (42), but because $\theta_{1\mathrm{TBA}} < \theta_{0\mathrm{DBA}}$, the TBA storage ring emittance can be smaller than the DBA emittance. For example, using the average TBA magnet bend angle $\overline{\theta}_{\mathrm{TBA}} = (2\theta_{1\mathrm{TBA}} + \theta_{2\mathrm{TBA}})/3 = \theta_{0\mathrm{DBA}}$, we obtain [26]

$$\varepsilon_{\mathrm{TBA}} = \left(\frac{3}{2+\sqrt[3]{3}}\right)^3 \varepsilon_{\mathrm{DBA}} \approx 0.66\varepsilon_{\mathrm{DBA}}\,.$$

In the general case of the MBA, the expression for the minimum emittance of an isomagnetic lattice coincides with (42):

$$\varepsilon_{\mathrm{MBA}} \approx \frac{C_q\gamma^2}{J_x}\,\frac{\theta_{1\mathrm{MBA}}^3}{4\sqrt{15}}\,,$$

where the bend angle of an edge magnet $\theta_{1\mathrm{MBA}}$ in a ring with N superperiods can be found from the relation

$$2\theta_{1\mathrm{MBA}} + (M-2)\,\theta_{2\mathrm{MBA}} = \frac{2\pi}{N}\,.$$

The FODO[2] cell is a simple, compact magnet cell using the minimum number of elements (Fig. 7). Because the minima of the horizontal betatron and dispersion functions are located outside the magnet (in a defocusing lens), the F_{FODO} factor is large compared with the F factors of the lattices described above. However, for a storage ring with a fixed length, the number of magnets in the FODO configuration is larger than in other lattices with the same length (due to the FODO compactness) and hence the emittance can be small due to the small value of θ^3.

In the thin-lens approximation (the focal length f is much larger than the lens length), the F_{FODO} factor (44) has the form [27]

$$F_{\mathrm{FODO}} = \frac{1-(3/4)\,\sin^2\mu_x}{\cos\mu_x\,\sin^3\mu_x}\,, \tag{50}$$

where μ_x is the phase over half the cell length. The F_{FODO} dependence on the full increase in the betatron phase per cell, $2\mu_x$, is shown in Fig. 8.

The minimum value $F_{\mathrm{mFODO}} \approx 1.2$ is attained at $2\mu_x \approx 137^\circ$. For the full increase in the betatron phase per cell, $2\mu_x \approx 90^\circ$ $F_{\mathrm{FODO}_{90}} \approx 2\sqrt{2}$.

There is some conventionality in the magnet lattice classification. For example, the MBA cell shown in Fig. 6 is

[2] FODO (Focusing–Open space–Defocusing–Open space) is a cell that consists of two quadrupole magnets with a horizontal focusing field (F) and horizontal defocusing field (D). After each magnet, there is an open space (O) with no magnetic field.

Table 1. Minimum emittance for various magnet lattices.

Lattice	F	Optimization conditions
FODO_{90}	$\approx 2\sqrt{2}$	$2\mu_x = 90^\circ\,,\quad \dfrac{f}{L} = \dfrac{1}{\sqrt{2}}$
$\mathrm{FODO}_{\min}$	≈ 1.2	$2\mu_x \approx 137^\circ$
$\mathrm{DBA}_{\min}$	$\dfrac{1}{4\sqrt{15}}$	$\eta_0 = \eta_0'\,,\quad \beta_{x0} = L\sqrt{\dfrac{12}{5}}\,,\quad \alpha_0 = \sqrt{15}$
TBA	$\dfrac{1}{4\sqrt{15}}\left(\dfrac{3}{2+\sqrt[3]{3}}\right)^3 \approx \dfrac{0.66}{4\sqrt{15}}$	$\rho_1 = \rho_2\,,\quad L_2 = \sqrt[3]{3}L_1$
MBA	$\dfrac{1}{4\sqrt{15}}\left(\dfrac{M}{2+(M-2)\sqrt[3]{3}}\right)^3$	$\rho_1 = \rho_2\,,\quad L_2 = \sqrt[3]{3}L_1$
TME	$\dfrac{1}{12\sqrt{15}}$	$\eta_{\min} = \dfrac{L\theta}{24}\,,\quad \beta_{x\min} = \dfrac{L}{2\sqrt{15}}$

precisely a FODO lattice in which the defocusing lens and the bending magnet are combined. Presumably, such a lattice was first used due to its compactness in the VEPP-3 and VEPP-4 storage rings at the BINP SB RAS [28].

Table 1 summarizes the results of emittance optimization in various magnet lattices. Key explanations and the notation are given in the text. We recall that TBA and MBA are combined cells, which use magnets with different lengths (an isomagnetic field is assumed); therefore, in order to compare different lattices, the F factor is given for the average over the magnet bend angle, as was explained above.

For all lattices except FODO, the minimum emittance was obtained under the condition that the superperiod provides an achromatic bend. If we allow the dispersion function to be nonzero in straight sections, then the emittance can be further reduced by a factor of 1.5–2. In this case, we should additionally take into account that due to the increase in the effective beam size [see (35)], the brightness of the undulator radiation can decrease and, if there is a wiggler with a strong field installed in the straight section, the emittance can even increase (see Section 4.3).

The first dedicated synchrotron radiation sources were still using the FODO lattice [Photon Factory (Japan) and Double Ring Store — DORIS (Germany)]. With the emittance reduction methods being developed, various versions of the DBA and TBA lattices are becoming popular. Examples of DBA SR sources are the Elettra (2 GeV, Italy) or the Advanced Photon Source — APS (7 GeV, USA). TBA SR sources are the Pohang Light Source — PLS (S. Korea), the Advanced Light Source — ALS (USA), and the Taiwan Photon Source — TPS (Taiwan). In storage rings built over the last few years using the MBA lattice, the emittance is significantly lower than 1 nm as, for example, in MAX IV (Sweden) or ESRF Extremely Brilliant Source — EBS (France).

In concluding this section, we note that the above minimum emittance values cannot be achieved in practice, because that would require too rigid focusing, fraught with various technological and dynamical problems. It is the developer's skill that defines how close one can get to these minimum values. For example, a 7 GeV APS storage ring provides $\varepsilon_{\mathrm{real}}/\varepsilon_{\min} \approx 3.6$ and the Elettra SR source at Trieste provides $\varepsilon_{\mathrm{real}}/\varepsilon_{\min} \approx 1.4$ (here, magnets with a transverse field gradient are used, which we consider in Section 4).

References to electronic resources that describe various SR sources can be found in [29].

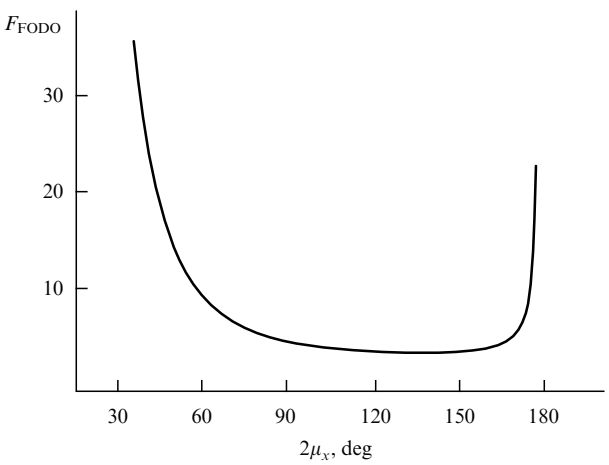

Figure 8. F_{FODO} [see Eqn (50)] versus the full increase in the betatron phase $2\mu_x$ per FODO cell.

4. The use of special magnets

After optimizing the magnet lattice, one can additionally reduce the emittance by using special magnets, like those with a transverse or longitudinal field gradient, as well as magnetic wigglers (periodic magnetic systems), which create an alternating field on the beam orbit.

4.1 Magnet with a transverse field gradient

Magnets with a transverse field gradient $G = \partial B_y/\partial x$ have a double effect on the emittance. The appearance of the gradient changes the behavior of the lattice functions entering $H(s)$ in (27), and optimization for TME then provides the minimum $H(s)$ averaged over the magnet:

$$\langle H_{\mathrm{TME}}(K)\rangle \approx \langle H_{\mathrm{TME}}(0)\rangle \times \left(1 - \frac{3}{70}KL^2 + \frac{17}{19600}K^2L^4 + \ldots\right), \qquad (51)$$

where $K = G/(B\rho)$ is the reduced focusing coefficient and L is the magnet length. As a result, the mean dispersion invariant increases for a defocusing magnet ($K < 0$) and decreases for a focusing one ($K > 0$).

The other, stronger, effect is related to the change in the radiation integral I_4, Eqn (23), which determines horizontal and longitudinal damping decrements. The possibility of reducing the horizontal emittance by using gradient magnets was first pointed out by Vignola [30]. In the approximation of a small bending angle of a dipole, $\theta \ll 1$,

$$J_x \approx 1 - \frac{1}{6} KL^2 + \frac{1}{180} K^2 L^4 + \dots . \tag{52}$$

After comparing the coefficients in (51) and (52), it is easy to see that the net effect $\varepsilon_x \sim \langle H \rangle / J_x$ is a decrease in emittance for a defocusing magnet, and an increase for a focusing one. As we have mentioned, the increase in the horizontal damping decrement leads to a decrease in the longitudinal decrement; therefore, in practice, we obtain values $J_x \sim 1.5-2.0$. A positive feature of a defocusing bending magnet is the reduction in the number of vertically focusing quadrupole lenses, which makes the magnet lattice more compact.

Defocusing bending magnets are used in SR sources such as Elettra ($B = 1.21$ T, $G \approx -2.86$ T m^{-1}) [31], ALS ($B = 1$ T, $G \approx -4$ T m^{-1}) [32], and PLS II ($B = 1.45$ T, $G \approx -4$ T m^{-1}) [33]. The gradient is small compared with the gradient in quadrupole lenses, but the magnet length of ~ 1 m provides noticeable vertical focusing.

4.2 Magnet with a longitudinal field gradient

To obtain a low emittance, the horizontal betatron and dispersion functions should be minimal on some azimuth of the bending magnet and increase as in open space outside it (neglecting the weak focusing $\sim \rho^{-2}$). Along with these functions, $H(s)$ also increases. But because the integrand in (29) includes the term $H(s)/|\rho^3|$, the increase can be compensated by making the field $B \sim 1/\rho$ large in the region where $H(s) = \min$, and decreasing as the dispersion invariant increases. The integral I_5 and the resulting emittance should then be lower than those in the isomagnetic case. These considerations are valid for any lattice, but for simplicity and clarity we consider only the TME lattice in what follows ($H(s)$ reaches its minimum in the magnet center).

Using magnets with a longitudinal gradient in order to additionally decrease the emittance was first proposed by Wrulich in 1992. This proposal remained unpublished at that time and the corresponding article [34] appeared only in 2007. Numerical optimization of a magnet with a longitudinally inhomogeneous field was discussed in 2002 [35]. The orbit curvature changed from the center to the edge of the magnet according to the equation $1/\rho(s) = b/(1 + as)^l$, where a and b are constants. It was shown that the emittance reaches its minimum for $l \approx 1$, that is, for an almost linear increase in the magnet bend radius. With an unlimited maximal field, the emittance could be made arbitrarily small.

The minimum emittance for various field profiles along a magnet was studied analytically and numerically in [36–40]. The problem that arises is that the optimization procedure turns out to be very laborious, resulting in complicated expressions, which can be investigated only numerically. However, expanding the exact expressions in a series in the magnet bending angle allows obtaining simple dependences that can be used to identify general trends and give a recommendation for the parameters of the magnet with longitudinal field variation. Below, we follow the considerations in [41, 42].

We consider a magnet in which the curvature radius is minimal in the center ρ_c and increases linearly at the edges to a value ρ_s, as shown in Fig. 9:

$$\rho(s) = ks + \rho_c = \frac{2(\rho_s - \rho_c)}{L} s + \rho_c , \tag{53}$$

where k is the longitudinal gradient and L the full length of the magnet. The field has its maximum B_c in the center and decreases hyperbolically to B_s at the magnet edges.

The full bending angle in such a field is

$$\theta = \frac{2 \ln(\rho_s/\rho_c)}{k} = \frac{2y}{k} .$$

Substituting (53) in (1) and (8), calculating the lattice functions and the dispersion invariant, and optimizing equilibrium emittance (30), we obtain [41]

$$\varepsilon_{\mathrm{LR\,min}} = \frac{C_q \gamma^2}{J_x} \frac{\theta^3}{12\sqrt{15}} \frac{3\sqrt{15} \exp(-y)}{y^3 \left(\exp(y) - 1\right)} \left(\frac{A(y)\, B(y)}{\exp(2y) - 1} \right)^{1/2} , \tag{54}$$

where $y = k\theta/2 = \ln(\rho_s/\rho_c) = \ln(B_c/B_s)$, and two auxiliary functions are expressed as

$$A = (4y - 23) \exp(4y) + 8(y + 5) \exp(3y) - (y^2 + 12y + 10) \exp(2y) - 8 \exp(y) + 1 ,$$

$$B = 2 \exp(2y) - y^2 - 2y - 2 .$$

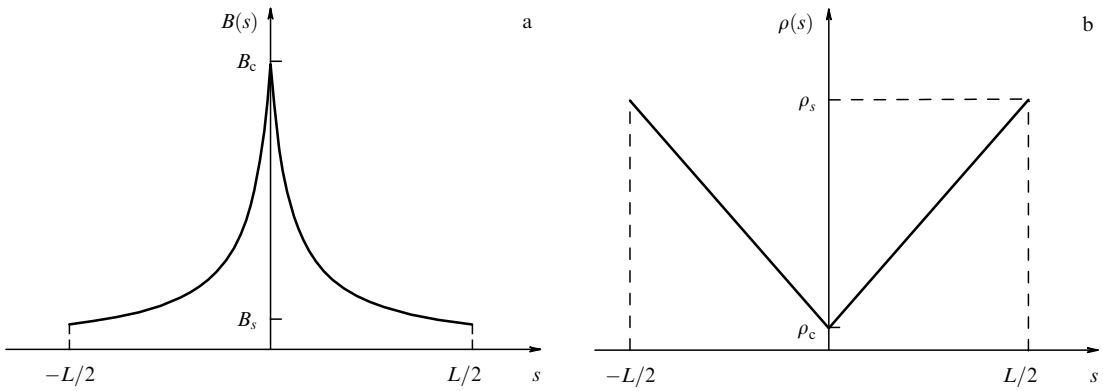

Figure 9. Profiles of (a) the magnetic field and (b) the bending radius for a magnet with a longitudinal gradient k.

The obtained expressions are quite cumbersome for analysis, but by expanding them in series in $\theta < 1$, we find a simple dependence that shows how the minimum emittance changes compared with the minimum emittance in a homogeneous field, Eqn (46):

$$\varepsilon_{\mathrm{LR\,min}} \approx \varepsilon_{\mathrm{TME}} \left(1 - \frac{9k\theta}{32} + \frac{2337k^2\theta^2}{71680} - \ldots\right). \tag{55}$$

Here, $\varepsilon_{\mathrm{TME}}$ was calculated for $B_{\mathrm{TME}} = B_{\mathrm{c}}$ and $\theta_{\mathrm{TME}} = \theta$. It turns out that the additional reduction in the emittance depends only on one parameter, $y = \ln(B_{\mathrm{c}}/B_s)$. Figure 10 shows the relative decrease in the minimum emittance for a magnet with the curvature radius increasing linearly with y.

For the considered magnet, the emittance decrease is limited by the maximal field value in the center. For a reasonable value of the gap between the magnetic poles (several centimeters), using modern superconducting technologies, we can presumably obtain $B_{\mathrm{c}} \sim 10$ T [43]. It may seem that for a field reaching zero values at the edges, $B_s \to 0$ ($y \to \infty$), an arbitrarily small emittance can be obtained. But if the bending angle and the field at the center are fixed, the magnet length would increase ($B_s \to 0$, $L \to \infty$), which is unacceptable due to the increase in the storage ring perimeter.

Two other models of the longitudinal variation of the magnetic field were considered in [42]. For a sandwich-dipole (SD) field (strong in the center and weak at the edges), there is a principal limitation for the emittance reduction: $\varepsilon_{\mathrm{SD}} \approx 0.22\,\varepsilon_{\mathrm{TME}}$, where $\varepsilon_{\mathrm{TME}}$ corresponds to a magnet with a homogeneous field equal to the central field of the SD magnet and with the bending angle equal to the full bending angle of a gradient magnet. When approaching this limit, the central field grows infinitely, while the edge field decreases to zero, and the bending angles of the central and edge magnets turn out to be equal.

Another popular model of a magnet with a longitudinal field gradient combines the properties of the two models described above: the field in this magnet is constant in the center and decreases hyperbolically at the edges. The exact solution for the minimum emittance is very cumbersome (the expression is several dozen lines long), but the expansion in a series in $y = \ln(B_{\mathrm{c}}/B_s)$ allows interpreting the results quite easily. The resulting series is similar to (54), but its coefficients are not constant, instead being functions of the ratio between the decreasing field bending angle and the full angle θ:

$$\varepsilon_{\mathrm{LRFT\,min}} \approx \varepsilon_{\mathrm{TME}} \left(1 + a_1(p)\,y + a_2(p)\,y^2 + a_3(p)\,y^3 + \ldots\right),$$

where $p = \theta_s/\theta$, and $a_i(p)$ are polynomials. For example,

$$a_1(p) = -\frac{1}{32}\,p\left(5p^4 - 30p^3 + 74p^2 - 96p + 56\right).$$

Calculations show that the optimal value providing the minimum emittance is $p \approx 0.5$.

The use of magnets with a longitudinal field gradient is a very promising method for the additional emittance reduction. For example, in the ESRF upgrade project, dipoles are used in which the magnetic field changes along the orbit from 0.65 T to 0.16 T.

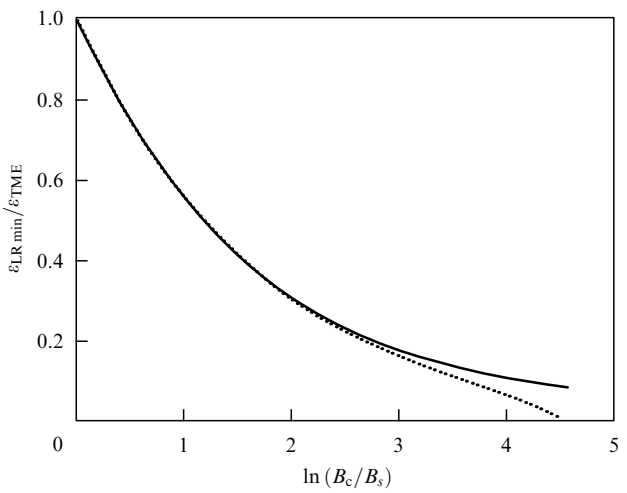

Figure 10. Relative minimum emittance for a magnet with a linear increase in the curvature radius. Solid curve corresponds to exact solution (54), while the dashed one is approximation (55).

4.3 Emittance reduction using wigglers

Emittance reduction using periodic magnetic systems — wigglers — was considered in detail in [44]. Some of these results are presented in this section.

A wiggler consists of a set of alternating magnets, which increases the radiation reaction force and under certain conditions leads to a decrease in the beam emittance. If we write the radiation integrals separately for the ring magnets and for the wiggler, $I_n = I_{n0} + I_{n\mathrm{w}}$, then the relative emittance change can be expressed as

$$r_\varepsilon = \frac{\varepsilon_{x\mathrm{w}}}{\varepsilon_{x0}} = \frac{1 + I_{5\mathrm{w}}/I_{50}}{1 + I_{2\mathrm{w}}/I_{20}}. \tag{56}$$

The vertical field along the wiggler axis z (we consider only the regular region and ignore the contribution of edge poles) can be described in the cosine model framework,

$$B_y(x = y = 0, z) = B_{\mathrm{w}} \cos(k_{\mathrm{w}} z) = B_{\mathrm{w}} \cos\left(\frac{2\pi}{\lambda_{\mathrm{w}}}\,z\right),$$

where B_{w} and λ_{w} are the amplitude and the period of the magnetic filed. Using this model, an estimate can be found for the radiation integral in a wiggler with the number of periods N, the length $L_{\mathrm{w}} = N\lambda_{\mathrm{w}}$, and the mean value of the horizontal betatron function $\beta_x(z) = \bar{\beta}_x$:

$$I_{2\mathrm{w}} = \frac{1}{2}\,h_{\mathrm{w}}^2 L_{\mathrm{w}}, \quad I_{5\mathrm{w}} \approx \frac{8}{15}\,N\theta_{\mathrm{w}} h_{\mathrm{w}}^2 \left(\frac{5\eta_{\mathrm{w}0}^2}{\bar{\beta}_x} + \bar{\beta}_x \theta_{\mathrm{w}}^2\right). \tag{57}$$

Here, $h_{\mathrm{w}} = 1/\rho_{\mathrm{w}} = B_{\mathrm{w}}/(B\rho)$ is the maximal curvature of the trajectory in the wiggler, $\theta_{\mathrm{w}} = h_{\mathrm{w}}/k_{\mathrm{w}}$ is the maximal deviation angle of the orbit from the wiggler axis, and $\eta_{\mathrm{w}0}$ is the dispersion function on the straight section of the storage ring in which the device is installed. In $I_{5\mathrm{w}}$, we show only the lowest-order terms in the angle $\theta_{\mathrm{w}} \ll 1$. The fifth integral in (57) reaches its minimum at $\eta_{\mathrm{w}0} = 0$. But because the dispersion function cannot be set precisely to zero in the straight section, it is reasonable to set a practical threshold below which the influence of the residual dispersion on the resulting emittance is considered small:

$$\eta_{\mathrm{w}0} \ll \frac{\bar{\beta}_x \theta_{\mathrm{w}}}{\sqrt{5}}.$$

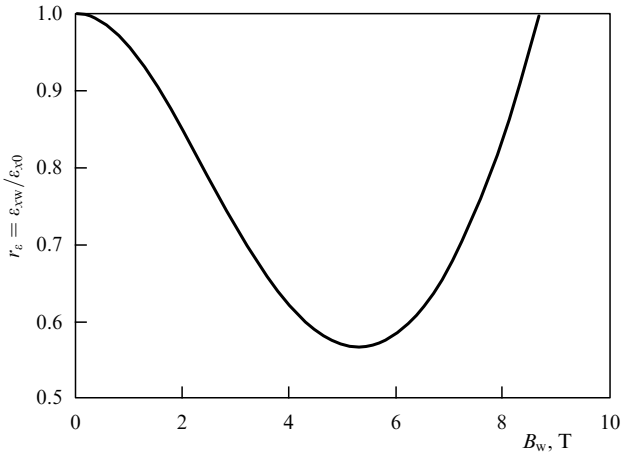

Figure 11. Relative variation of the beam emittance due to the wiggler influence.

Under this condition, the fifth radiation integral of the wiggler can be expressed as

$$I_{5w} \approx \frac{8}{15} N\theta_w^3 h_w^2 \bar{\beta}_x .$$

Substituting I_{5w} and I_{2w} in (56), we obtain

$$r_\varepsilon \approx \frac{1 + 8N\theta_w^3 h_w^2 \bar{\beta}_x/(15 I_{50})}{1 + h_w^2 L_w/(2 I_{20})} . \tag{58}$$

Figure 11 shows the typical dependence of the r_ε function in Eqn (58) on the wiggler field amplitude. For a given field period, when increasing its amplitude, the emittance first decreases due to the additional damping and then increases due to the enhancement of quantum induced oscillations. The minimum of the curve in Fig. 11 provides the amplitude of the wiggler field for which the emittance is minimal.

The wiggler influences not only the emittance but also other beam parameters, including the energy spread. For the cosine field model, the third radiation integral in Eqn (32) increases by

$$I_{3w} = \frac{4}{3\pi} h_w^3 L_w . \tag{59}$$

The intention is to make the magnetic wiggler field homogeneous in the horizontal direction, but the edge focusing of the poles leads to a modification of the vertical betatron function and to a shift of the vertical betatron frequency by

$$\Delta\nu_y = \frac{1}{8\pi} h_w^2 L_w \bar{\beta}_y , \tag{60}$$

where $\bar{\beta}_y$ is the vertical betatron function of the wiggler averaged over its length. To compensate these parasitic effects, the vertical betatron function in the wiggler is designed to be small, and special quadrupole lenses are used to compensate the vertical focusing variation.

Twenty damping wigglers developed and fabricated at the BINP SB RAS with a net length of 80 m, the period $\lambda_w = 0.2$ m, and the field amplitude $B_w = 1.5$ T resulted in a four-fold reduction in the horizontal emittance of the PETRA III (Positron–Electron Tandem Ring Accelerator III) SR source with the energy of 6 GeV, reaching a record small value $\varepsilon_x = 1$ nm [45].

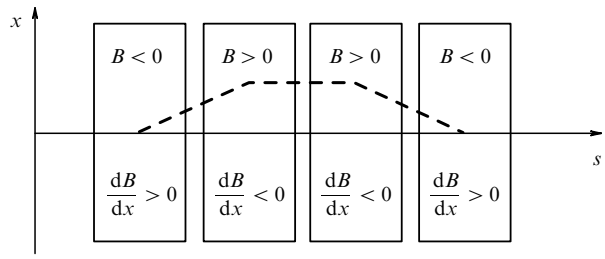

Figure 12. The Robinson wiggler. Dashed line schematically shows the beam orbit.

4.4 Robinson wiggler

In a storage ring that uses homogeneous-field magnets, the emittance can be decreased by redistributing the damping decrements (as was considered in Section 4.1) using the gradient wiggler proposed by Robinson [18].

The Robinson wiggler is a sequence of magnets in which the field and the gradient change such that their product is negative (Fig. 12). The field integral is chosen to be such that the beam orbit is not disturbed outside the wiggler. A device installed in the gap with a nonzero dispersion function creates a horizontal dimensionless damping decrement given by (22),

$$J_x \approx 1 - \frac{\bar{\eta}}{\pi |h_{w0}|} \int_0^{L_w} h_w(z)\, K_w(z)\, dz , \tag{61}$$

where $\bar{\eta}$ is the dispersion function averaged over the wiggler length, $|h_{w0}|$ is the orbit curvature modulus (the field of each pole has the same absolute value), and $K_w = (\partial B_y/\partial x)/(B\rho)$ is the reduced field gradient.

Using the Robinson wiggler at the Proton Synchrotron (PS) at CERN allowed reducing the horizontal emittance by 50% [46]. Currently, there are plans to install a gradient wiggler in the following SR sources: SOLEIL [3] (France) [47], TPS (Taiwan) [48], and Metrology Light Source — MLS (Germany) [49].

5. Problems of emittance reduction

Reaching limit values of the parameters is always accompanied by overcoming both technological and fundamental difficulties. A detailed description of such difficulties related to low-emittance storage rings would be too long. In this section, we briefly consider some of the main problems related to the beam dynamics. Technological difficulties related to the construction of low-emittance storage rings are discussed in examples in Section 6. Details can be found, e.g., in [50].

5.1 Chromatic correction and dynamic aperture

The coefficients in Eqns (1) and (2) depend on the particle energy; if it is different from the equilibrium value, $E = E_0 + \Delta E = E_0(1 + \delta)$, where $\delta = \Delta E/E_0 \ll 1$, the particle is focused differently than the equilibrium one, in accordance with

$$K_{x,y}(\delta) = \frac{G}{B\rho(1+\delta)} \approx K_{x,y}(0)(1 - \delta) .$$

[3] (French) Source Optimisée de Lumière d'Energie Intermédiaire du LURE (Laboratoire pour l'utilisation du rayonnement électromagnétique).

The focusing strength dependence on the energy, known as the chromaticity, can be regarded as a systematic error in the focusing coefficient,

$$\Delta K_{x,y}(s) \approx -K_{x,y}(s)\,\delta\,, \tag{62}$$

leading to the dispersion of betatron frequencies in the beam, a distortion of the optical functions, and limits on steady motion for a nonequilibrium particle, as well as other undesired effects. The betatron oscillation frequency can be expanded in a series in the particle energy deviation

$$\nu(\delta) = \nu_0 + \xi_1\delta + \xi_2\delta^2 + \ldots\,, \tag{63}$$

where

$$\xi_1 = \frac{\mathrm{d}\nu}{\mathrm{d}\delta} \tag{64}$$

is known as the linear natural chromaticity of the betatron frequency and can be estimated as (we omit the subscript in what follows)

$$\xi_{x,y} \approx -\frac{1}{4\pi}\oint K_{x,y}(s)\,\beta_{x,y}(s)\,\mathrm{d}s\,. \tag{65}$$

It can be seen from expression (65) that the tighter the focusing is (which is needed for the emittance reduction), the larger the storage ring chromaticity. Table 2 shows values of the natural chromaticity divided by the number of superperiods ($\xi_{x,y\mathrm{c}} = \xi_{x,y}/N_\mathrm{c}$) together with other parameters for three SR sources of different generations.

To compensate the chromaticity, sextupole lenses (SLs) are used, in which the field depends quadratically on the coordinates:

$$B_y(s) = \frac{1}{2}\,B''(s)(x^2 - y^2)\,,$$

$$B_x(s) = B''(s)\,xy\,, \quad B'' = \frac{\partial B_y}{\partial x^2}\,. \tag{66}$$

If a sextupole lens is placed in the azimuth where the dispersion function $\eta(s) \neq 0$, then because the horizontal displacement of the particle with nonequilibrium energy is given by [Eqn (6)]

$$x(s) = x_\beta(s) + \eta(s)\,\delta\,,$$

it follows that field (66) that acts on the particle can be represented (up to δ) as

$$B_y \approx (B''\eta)\,\delta x_\beta + \frac{B''}{2}\,(x_\beta^2 - y^2)\,,$$

$$B_x = (B''\eta)\,\delta y + B'' x_\beta y\,. \tag{67}$$

The first term in (67) depends on the betatron coordinate linearly and, similarly to (62), is an energy-dependent focusing correction,

$$\Delta K^{\mathrm{SL}}(s) = \frac{B''(s)}{B\rho}\,\eta(s)\,\delta = m(s)\,\eta(s)\,\delta\,,$$

which can be used for the linear chromaticity compensation in accordance with

$$\xi_{x,y}^{\mathrm{SL}} = \pm\frac{1}{4\pi}\oint\frac{B''(s)}{B\rho}\,\eta(s)\,\beta_{x,y}(s)\,\mathrm{d}s\,, \tag{68}$$

where the + sign corresponds to the vertical plane.

The smaller the emittance is, the tighter the focusing, the larger the chromaticity, the smaller the dispersion function, and the stronger sextupole lenses are needed to compensate the chromaticity. The maximal integral gradient of a sextupole lens at a second-generation SR source ANKA with the emittance $\varepsilon_x = 70$ nm is $B''L = 700 \times 0.1$ T m^{-1}, while for the fourth-generation SR source ESRF–EBS with $\varepsilon_x = 0.13$ nm, this is already $B''L = 1700 \times 0.2$ T m^{-1}.

Fabricating strong sextupole magnets is a complicated technological problem, but the main problem is related to the fact that the betatron oscillation equations become nonlinear (due to the second term in (6)). A nonlinear oscillator has important properties: anharmonicity (the appearance of a large, generally infinite, number of harmonics in the force) and nonisochronicity (the dependence of the oscillation period and frequency on the amplitude). Due to these properties, the increase in the amplitude would lead to a change in the particle oscillation frequency until it reaches either a strong low-order resonance or the region of overlapping weak high-order resonances, with the result that the regular motion becomes stochastic [51]. Both outcomes result in the collapse of the particle. The region of the initial parameters of betatron motion that corresponds to regular motion is called the dynamic aperture. A small dynamic aperture limits the particle lifetime and the injection efficiency.

Figure 13 shows the dynamic aperture of a small-emittance electron storage ring, obtained by simulating the particle motion in a nonlinear magnet lattice. The visualization is performed using a popular technique, frequency map analysis (FMA) [52], allowing regular and stochastic motion to be separated. The plot shows the set of initial parameters for the particles that are stable over a certain period of time (usually of the order of the damping time). The white region corresponds to an unstable particle and the shades of grey indicate the betatron frequency diffusion rate for a particle with given initial conditions. Strong frequency diffusion is characteristic of stochastic (unstable) trajectories. It is seen that the maximal horizontal coordinate (horizontal dynamic aperture) is $A_x = x_{0\,\max} \approx 15$ mm and the vertical one is

Table 2. SR radiation sources and their parameters.

Storage ring	Generation	Country	E, GeV	Π, m	ε_x, nm	N_c	$\xi_{x\mathrm{c}}/\xi_{y\mathrm{c}}$
ANKA*	2	Germany	2.5	110	70	8	−2/ − 1
Elettra	3	Italy	2.4	259	10	12	−3/ − 2
Sirius	4	Brazil	3	518	0.3	20	−6/ − 4

* Abbreviation from German Angströmquelle Karlsruhe.

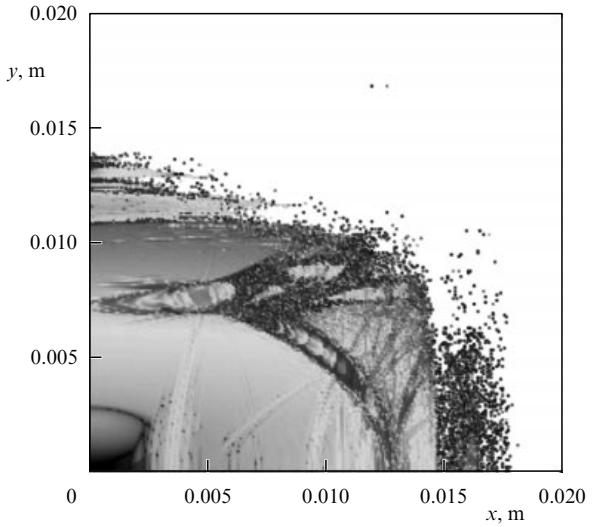

Figure 13. Example of a dynamic aperture image for a storage ring. Each point corresponds to the particle with initial conditions (x_0, y_0, $x'_0 = y'_0 = 0$), being stable over the horizontal damping time.

$A_y = y_{0\,\max} \approx 12$ mm. The uncertainty in the aperture size is related to the fact that the unstable motion region can contain isolated islands of stable trajectories, and there is therefore some uncertainty in the definition of the boundary between the stable and unstable motion regions. Different regions in Fig. 13 are related to nonlinear resonances, which satisfy the equation $m_x \nu_x(x_0, y_0) + m_y \nu_y(x_0, y_0) = n$, where $m_{x,y}$ and n are integer numbers. Close to the resonances, the share of the stochastic motion increases.

For a particle with a nonequilibrium energy, the dynamic aperture is usually smaller than for a particle with the equilibrium energy, which motivates introducing the dynamic energy acceptance — the energy deviation $\delta_{\max} = \Delta E_{\max}/E_0$ — for which the transverse dynamic aperture is larger than zero. The characteristic value of the dynamic acceptance is $\delta \sim \pm(1-5)\%$. A small acceptance leads to a short lifetime.

Limiting the dynamic aperture and the energy acceptance is one of the most serious problems for low-emittance storage rings, and many studies are related to this topic (see, e.g., [53–55] and the references therein). For theoretical estimates, various versions of the perturbation theory are used. Numerical modeling and optimization are performed using modeling programs, which solve the particle equations of motion (in the most general case, for three degrees of freedom) in the magnetic field of a storage ring with nonlinear components taken into account. Besides sextupole lenses, there are other sources of nonlinear perturbations, such as wigglers and undulators, errors in the magnetic element fabrication, and a field created by the space charge of the electron bunch.

5.2 Vertical emittance

For a planar storage ring, the vertical emittance determined by SR is very small. Because it is impossible to make the orbit ideally flat (due to magnetic field errors), the vertical emittance is in reality several orders of magnitude larger than that defined by expression (31). The main contribution is made by two effects: linear coupling of the betatron oscillations and excitation of the vertical dispersion function.

The coupling of betatron oscillations occurs when Eqns (1) and (2) contain terms depending on the second coordinate. This can happen when the quadrupole lenses on the ring are slightly tilted with respect to the beam axis, when there are solenoid fields, or when the beam is deflected vertically in sextupole lenses. The linear betatron coupling constant κ depends on the magnitude of the error in the magnetic element positioning, the closed beam orbit, and the closeness of betatron frequencies to the coupling resonance $\nu_x - \nu_y = n$. This changes the equilibrium emittance of the beam in accordance with

$$\varepsilon_x = \frac{1}{1+\kappa}\,\varepsilon_{x0}\,, \quad \varepsilon_y = \frac{\kappa}{1+\kappa}\,\varepsilon_{x0}\,, \tag{69}$$

where ε_{x0} is radiation emittance (30). In the case of full coupling $\kappa = 1$, $\varepsilon_x = \varepsilon_y = \varepsilon_{x0}/2$. In the opposite case $\kappa \ll 1$, which is characteristic of modern low-emittance electron storage rings, $\varepsilon_x \approx \varepsilon_{x0}$ and $\varepsilon_y \approx \kappa\varepsilon_{x0}$.

The horizontal dipole component of the field B_x acting on the particle leads to the appearance of the vertical dispersion function η_y, and the vertical emittance is formed by SR fluctuations as described in Section 2.2:

$$\varepsilon_y = C_q \gamma^2 \frac{I_{5y}}{J_y I_2}\,, \quad I_{5y} = \oint \frac{H_y(s)}{|\rho^3(s)|}\,\mathrm{d}s \approx \langle H_y \rangle\, I_3\,,$$

where $\langle H_y \rangle$ is the value averaged over the lattice. Then

$$\varepsilon_y \approx \frac{J_E}{J_y}\,\langle H_y \rangle\,\sigma_\delta^2\,.$$

The horizontal field arises due to the tilt of the dipole magnets with respect to the beam axis or due to the vertical offset of the quadrupole lenses. The betatron coupling (the tilt of the quadrupole lenses with respect to the beam axis and solenoid fields) also creates vertical dispersion even if the coupling source is located at an azimuth with nonzero horizontal dispersion.

In modern storage rings, the vertical emittance is determined by errors in the setup and in the fabrication of the magnetic element. The lower the horizontal emittance is, the tighter the focusing, the stronger the quadrupole and sextupole lenses, and the more rigorous the requirements for the accuracy of magnet fabrication and installation: characteristic values are of the order of micrometers. The orbit position is measured by electromagnetic sensors with a resolution of the order of 1 μm and is adjusted with weak correction magnets. The coupling of betatron oscillations is compensated by skew-quadrupole lenses rotated through 45° about the beam axis. This allows obtaining the vertical emittance at the level of $\varepsilon_y \approx 10^{-3}\,\varepsilon_{x0}$ or less (Table 3).

5.3 Intra-beam electron scattering

When experiencing oscillations, different particles of the same bunch can undergo elastic Coulomb collisions, during which

Table 3. Achieved emittance in SR sources [56].

Storage ring	Country	ε_x, nm	$\kappa = \varepsilon_y/\varepsilon_x$, %	ε_y, pm
ALS	USA	6.7	0.10	4–7
ASP	Australia	10	0.01	1–2
Diamond	England	2.8	0.07	2
ESRF	France	4	0.07	2.8
SOLEIL	France	3.7	0.10	4
SLS*	Switzerland	6	0.02	1

* Abbreviation of Swiss Light Source.

the change in the transverse momentum Δp_x is transformed into a change in the longitudinal one according to $\Delta p_s \sim \gamma \Delta p_x$. Because $\gamma \sim 10^3 - 10^4$, the change in the longitudinal momentum can be so large that both electrons find themselves outside the energy stability region. This phenomenon was first observed in a small storage ring ADA (Italian, Anello di Accumulazione) and was first explained [57] by Touschek and colleagues [58, 59]. It is now known as the Touschek effect.

Under the assumption that the beam is flat ($\varepsilon_y \ll \varepsilon_x$) and the transverse motion of the particle is nonrelativistic, the Touschek lifetime of the beam is [60, 61]

$$\frac{1}{\tau} = \frac{1}{N}\frac{\mathrm{d}N}{\mathrm{d}t} = \frac{r_\mathrm{e}^2 cq}{8\pi e\gamma^3\sigma_s}\left\langle \frac{D(\varepsilon^2)}{\sigma_x(s)\,\sigma_y(s)\,\sigma_{x'}(s)\,\delta_\mathrm{a}^2(s)}\right\rangle , \qquad (70)$$

where r_e is the classical electron radius, angular brackets denote averaging over the orbit, q and σ_s are the charge and the length of the bunch, $\sigma_{x,y}$ are the transverse dimensions, $\sigma_{x'}$ is the horizontal divergence, $\delta_\mathrm{a}(s) = \Delta p_\mathrm{a}(s)/p_0$ is the relative local energy acceptance, and

$$\varepsilon = \frac{\delta_\mathrm{a}(s)}{\gamma\sigma_{x'}(s)} ,$$

$$D(x) = \int_0^1 \left(u^{-1} - \frac{1}{2}\ln u^{-1} - 1\right)\exp\left(-\frac{x}{u}\right)\mathrm{d}u .$$

It follows from (70) that the Touschek beam lifetime rapidly decreases with a decrease in the particle energy and the bunch volume $V_\mathrm{b} \sim \sigma_s\sigma_x\sigma_y$, is inversely proportional to the beam intensity, $\tau \sim q^{-1}$, depends on the betatron coupling constant as $\tau \sim \sqrt{\kappa}$, and requires a large energy acceptance. This last is determined either by the longitudinal dynamics (the size of the synchrotron oscillation stability region) or by the transverse one, because an abrupt change in the particle energy due to a collision excites betatron oscillations (as in the case of emission of quanta) with an offset, which can overcome the transverse aperture.

If the particles in the bunch are scattered by a small angle and the variation of the longitudinal momentum is not large enough for them to be destroyed, such intra-beam scattering (multiple Touschek effect) leads to an increase in the beam emittance and energy spread in accordance with

$$\frac{\mathrm{d}\varepsilon_{x,y}}{\mathrm{d}t} = \frac{2}{T_{x,y}}\,\varepsilon_{x,y} , \quad \frac{\mathrm{d}\sigma_\delta}{\mathrm{d}t} = \frac{1}{T_\delta}\,\sigma_\delta ,$$

where $T_{x,y,\delta}$ is the rise time for the corresponding degree of freedom. Emittance growth due to collisions inside the bunch accompanied by abrupt changes in the particle energies is reminiscent of quantum diffusion due to SR. The difference lies in the fact that for the radiation, the result does not depend on the local bunch size, while for the scattering, on the contrary, it does: increasing the beam size leads to an increase in the collision rate. Therefore, the calculation of $T_{x,y,\delta}$ turns out to be quite cumbersome [62, 63]. The leading dependence on the bunch parameters has the form [64]

$$\frac{1}{T_{x,y,\delta}} \propto \frac{q}{\gamma^4\varepsilon_x\varepsilon_y\sigma_s\sigma_\delta} , \qquad (71)$$

which means that in the same manner as for the Touschek lifetime, there is a (strong) dependence on the energy, volume, and current of the bunch.

Taking the radiation damping with the time τ_x into account results in the following modification of the emittance evolution:

$$\frac{\mathrm{d}\varepsilon_x}{\mathrm{d}t} = -\frac{2}{\tau_x}\,(\varepsilon_x - \varepsilon_{x0}) + \frac{2}{T_x}\,\varepsilon_x ,$$

where ε_{x0} is the radiation emittance. The condition $\mathrm{d}\varepsilon_x/\mathrm{d}t = 0$ results in a new equilibrium emittance, which takes the synchrotron radiation and the intra-beam scattering into account:

$$\varepsilon'_{x0} = \frac{\varepsilon_{x0}}{1 - \tau_x/T_x} .$$

The vertical emittance is still related to the horizontal emittance through the betatron coupling constant.

Because the rise time of the bunch phase volume due to particle scattering depends on the phase volume itself, the process of its calculation is iterative. The same is valid for the Touschek lifetime: the growth of the emittance due to the multiple scattering increases the lifetime (because the density of particles in the bunch decreases), but the increase in the energy spread reduces it (for a constant energy acceptance).

Intra-beam scattering is a serious limiting factor for low-emittance storage rings. Starting from some emittance value, precisely this mechanism (which of course depends on the bunch current) determines the beam lifetime.

The intra-beam scattering can be reduced by increasing the beam energy, enhancing the radiation damping using wigglers, lengthening the bunch, or introducing a strong betatron coupling, which decreases the particle density in the bunch.

5.4 Space charge

Every electron experiences electromagnetic action from all other particles in the bunch. The strength of the space charge is connected with the simultaneous action of the electric and magnetic fields. For example, for the vertical coordinate, we can write

$$\gamma m\ddot{y} = e(E_y + \beta c B_x) .$$

Replacing the independent time variable t with the arc length $s = \beta ct$,

$$\ddot{y} = \beta^2 c^2 y'' ,$$

and using the relation between the horizontal component of the magnetic field and the vertical component of the electric field,

$$B_x = -\frac{E_y}{\beta c} ,$$

we can obtain the equation of particle motion

$$y'' = \frac{eE_y}{\beta^2\gamma^3 mc^2} . \qquad (72)$$

For a normal particle distribution, the electric field depends on the coordinates nonlinearly [65]. However, close to the beam axis, we can use the linear approximation

$$E_y \sim \frac{e\lambda}{2\pi\varepsilon_0}\frac{y}{\sigma_y(\sigma_x + \sigma_y)} , \qquad (73)$$

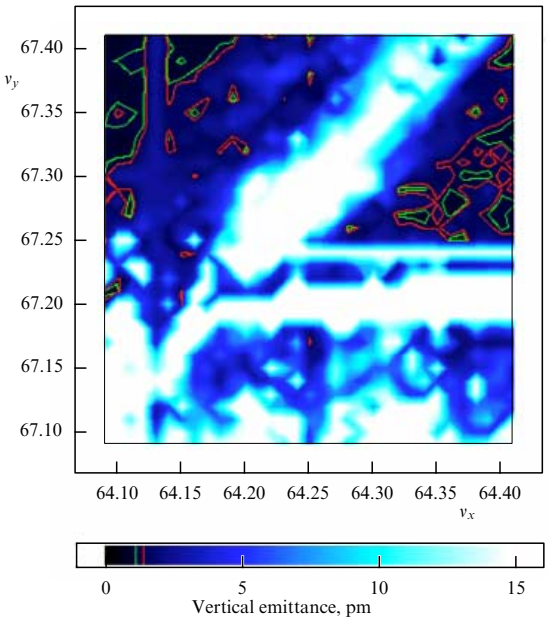

Figure 14. Vertical emittance of an electron bunch at the ILC damping ring versus the operating point of the betatron frequencies with the space charge taken into account. The dark region corresponds to the design value of the emittance, 2 pm. The vertical emittance is much larger in the bright regions ($\sim 10-15$ pm).

where $\lambda = N/(\sqrt{2\pi}\sigma_z)$ is the peak linear density of particles and ε_0 is the permittivity of the vacuum. On the one hand, the actions of the electric and magnetic fields in the relativistic case almost fully compensate each other, and hence the force in (72) is suppressed as $\sim \gamma^{-3}$. On the other hand, the magnitude of the electric field is inversely proportional to the product of the transverse beam sizes, $\sim 1/(\sigma_x\sigma_y)$, and can be quite large in the case of an extremely small emittance.

The space charge field leads to a growth of the emittance similarly to the increase in the transverse size of the bunch for head-on beams (beam blowup), which limits the luminosity. These effects are connected with the appearance and interaction of a large number of resonances (due to the nonlinear nature of the space charge forces) and are poorly described theoretically; the investigations are performed using computer simulations. Figure 14 shows the results of such simulation for one type of beam accumulator cooler ring at the International Linear Collider (ILC) with the vertical emittance of 2 pm [66].

We can see from Fig. 14 that in the vicinity of some resonances (described by lines in the betatron frequency plane), the space charge can significantly increase the vertical emittance. Despite the absence of a theory that would predict the emittance change due to the space charge, the degree of influence of the latter can be estimated in the same manner as is done in the case of the effects of beam collision in colliders using the incoherent shift of the betatron frequency. For this, we note that substituting (73) in (72) yields a linear differential equation similar to the betatron oscillation equation. Using it, we easily estimate the correction to the betatron frequency induced by the space charge (assuming that its influence is small):

$$\Delta\nu_{x,y} = -\frac{1}{4\pi}\frac{2r_e}{\gamma^3\beta^2}\oint\frac{\lambda\beta_{x,y}}{\sigma_{x,y}(\sigma_x+\sigma_y)}\,\mathrm{d}s\,. \qquad (74)$$

Numerical and experimental investigations of collision effects show that the beam blowup occurs if the space charge parameter is $\Delta\nu_{x,y} \sim 0.1$.

5.5 Coherent instabilities

An intensive electron bunch induces an electromagnetic field in the cavities of a vacuum chamber, which interacts with the particles of the same or another bunch. Such collective interaction can lead to beam instabilities or change the parameters (lengthen the bunch, increase the energy spread, etc.). Two factors emphasize some coherent effects in ultralow-emittance storage rings. The first is the small (due to the small value of the dispersion function) momentum compaction factor α, Eqn (34), and hence a short bunch according to (33). The shorter the bunch, the stronger the beam interaction with the environment can be in principle, because the spectrum of electromagnetic oscillations induced by the beam in the vacuum chamber broadens. A small value of α decreases the threshold current for single-bunch instabilities. For example, the average current in the bunch for the longitudinal microwave instability threshold is expressed as [67]

$$I_b \leqslant \frac{\sigma_{z0}}{R}\frac{\sqrt{2\pi}\,\alpha E/e}{|z_{\|}/n|_{\mathrm{eff}}}\left(\frac{\sigma_E}{E}\right)^2,$$

where R is the mean storage ring radius, σ_{z0} is the bunch length for a zero current, and $|z_{\|}/n|_{\mathrm{eff}}$ is the effective longitudinal impedance. As the bunch current exceeds the threshold value, both the length and the energy spread of the bunch increase with the beam intensity.

The second factor is the narrow vacuum chamber due to small-aperture quadrupole lenses providing strong focusing. A transverse multibunch instability can be excited due to the interaction of the beam with a resistive impedance of the vacuum chamber walls (resistive wall instability). The rise time of this instability is given by

$$\tau^{-1} \propto \frac{\overline{\beta}\omega_0 I}{Eb^3}\,,$$

where $\overline{\beta}$ is the average value of the betatron function, $\omega_0 = 2\pi f_0$, f_0 is the circulation frequency, and b is the characteristic transverse size of the vacuum chamber. It is clear that this type of instability is sensitive to the vacuum chamber size. The small mean value of the betatron functions (especially for the MBA lattice) also contributes to the development of this instability.

The unwanted collective effects can be eliminated by decreasing the vacuum chamber impedance using a relatively low-frequency accelerating system ($\sim 100-300$ MHz) that provides a large bunch length. The bunch length can be additionally increased using passive third-harmonic resonators, which flatten the potential well of the synchrotron motion. Fast feedback systems can also be used.

6. Paving the way to the diffraction limit

The wave character of radiation imposes a limitation on the spatial Δx and angular $\Delta\psi$ sizes of the source with a wavelength λ in accordance with $\Delta x \sim \lambda/\Delta\psi$ [68]. This means that even for a point-like electron, the emittance is limited by diffraction effects at the level of $\varepsilon_r \approx \Delta x\,\Delta\psi \sim \lambda$. For coherent undulator emission with a Gaussian distribu-

tion of the power density, the radiation emittance is expressed as [69]

$$\varepsilon_{\rm r} = \frac{\lambda}{4\pi}\,. \tag{75}$$

Achievements in the last decade in the calculation and optimization of cyclic accelerators, technologies for the development of various systems, beam control, and precise measurements of beam parameters have led to devices with the electron beam emittance comparable to the radiation emittance value. For estimates, it is common to use $\lambda \sim 1$ Å, which corresponds to $\varepsilon_x \sim \varepsilon_{\rm r} \sim 10$ pm. Such devices are known as diffraction-limited light sources (DLLSs) [70]; while these devices will hardly be realized in the nearest future, they help in finding technological solutions for ultralow emittances by investigating and overcoming the arising problems.

The first steps toward the diffraction limit were made in 2016 at Lund University with the launch of the first fourth-generation SR source MAX IV and in 2015 in Grenoble with the start of the ESRF–EBS project realization. Because these devices are examples for future projects and at the same time are test sites for new ideas and technologies, we briefly describe their main features. The parameters of MAX IV and ESRF–EBS are given in Table 4.

6.1 MAX IV synchrotron radiation source

The Max IV accelerating facility includes two rings with the maximum energies 1.5 GeV and 3 GeV [71]. The storage ring with a length of 528 m contains 20 superperiods of the 7BA lattice shown in Fig. 15.

Defocusing dipoles redistribute the damping decrements and lower the emittance by making the ring shorter due to the smaller number of quadrupoles. Central magnets of the 7BA cell rotate the beam by 3°, while the edge magnets, which set the dispersion function to zero, rotate it by 1.5 deg. As a result, the hard radiation from the main magnets is not transmitted to the straight sections and does not heat the vacuum chamber with installed superconducting devices.

The chromaticity correction (through the third order), as well as the optimization of the dynamic aperture and the energy acceptance, is performed by five families of sextupole lenses and three families of octupole lenses, which reduce the

Table 4. Main parameters of MAX IV and ESRF–EBS.

Parameter	MAX IV	ESRF – EBS
Lattice	7BA	HMBA***
E, GeV	3	6
Perimeter Π, m	528	844
Maximal current $I_{\max}$, mA	500	200
RF system frequency $f_{\rm RF}$, MHz	100	352
Number of straight sections*	20 (19)	32 (30)
Betatron frequencies ν_x, ν_y	42.2; 16.3	75.6; 27.6
Natural chromaticity ξ_x, ξ_y	−50; −50.2	−100; −84
Momentum compaction factor α	3.06×10^{-4}	0.87×10^{-4}
Horizontal decrement J_x	1.85	1.53
Horizontal emittance** ε_{x0}, pm	320	132
Energy dispersion σ_δ	7.7×10^{-4}	9.5×10^{-4}
Energy loss per revolution U_0, keV	364	3300

* Numbers in brackets denote the number of gaps for the installation of wigglers or undulators.
** Emittance without taking the intra-beam scattering and wigglers into account.
*** Hybrid MBA.

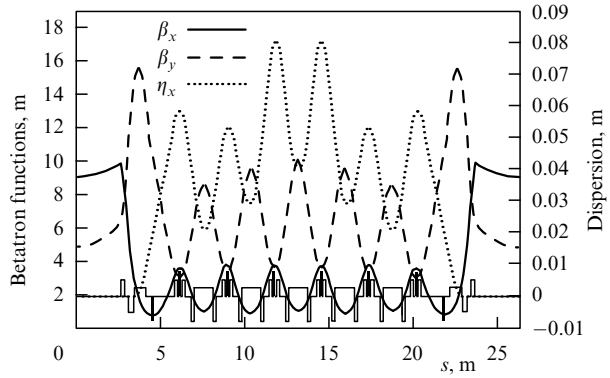

Figure 15. Optical functions of the MAX IV superperiod.

betatron frequency dependence on the amplitude. The choice of nonlinear elements was made after performing thorough computer simulations. Focusing lenses between the magnets are divided into two parts, and a sextupole is installed between them, located at the maximum of $\eta(s)$ and $\beta_x(s)$. As a result, at the center of the straight section, the dynamic aperture is $A_x \times A_y \approx 9 \times 2$ mm^2 for the energy acceptance $(\Delta p/p_0)_{\max} = \pm 4.5\%$, which provides quite a long beam lifetime and an effective injection.

For a zero current, the MAX IV emittance is $\varepsilon_{x0} =$ 320 pm. For a maximum current of 500 mA and a natural bunch length of 10 mm, the intra-beam scattering increases the emittance by 45%. Three passive third-harmonic resonators lengthen the bunch to 54 mm and reduce the scattering influence, resulting in the emittance $\varepsilon_{x0} = 370$ pm. Damping wigglers (for which either two superconducting wigglers with a field of 3.5 T or four devices with permanent magnets and a field of 2.2 T are considered) decrease the emittance to $\varepsilon_x = 220$ pm for the 500 mA current. Simulations predict a Touschek lifetime > 25 h. Moreover, the emittance reduction using wigglers increases the lifetime, because the horizontal momentum of the particle becomes so small that after the collision the longitudinal momentum turns is much less than the acceptance. The vertical emittance reaches the diffraction value ($\varepsilon_y = \varepsilon_{\rm r} = \lambda/(4\pi) = 8$ pm) for the betatron coupling constant $\kappa \approx 2{-}2.5\%$, which is the design value of the project.

For compactness, the magnetic elements are integrated into a single block (Fig. 16), which contains a dipole and several quadrupole, sextupole, octupole, and correction magnets, as well as beam position sensors [72]. The yoke that closes the magnetic flux is simultaneously a rigid bearing body, and hence there is no need for complicated precision stands. With careful processing and assembling in the laboratory, this construction allows obtaining a relative accuracy of adjacent element placing better than ±10 μm [73], which is unachievable in the case of individual installation of these magnets on the ring.

The emittance reduction is provided by strong focusing. The required maximal values of the lens gradients are $G = B' \approx 40$ T m^{-1} for quadrupoles and $B'' \approx 4000$ T m^{-2} for sextupoles, and $B''' \approx 40$ kT m^{-2} for octupoles, and they can be obtained only for a small aperture; therefore, the gap between the bending magnet poles is 28 mm and the inscribed diameter of the lenses is 25 mm.

The vacuum system must guarantee a low pressure of the residual gas ($\sim 10^{-9}$ Torr), but the gas conduction of a

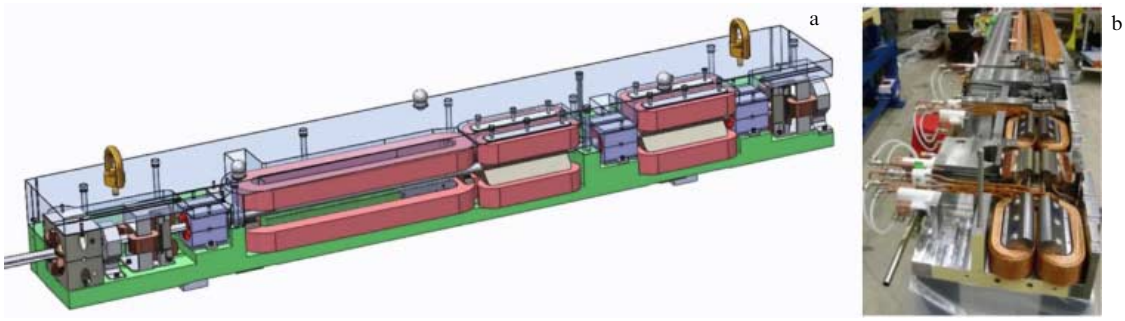

Figure 16. MAX IV magnets combined in a single block: (a) sketch, (b) photograph (with the upper half removed).

chamber with an inner diameter of 22 mm is small, and the use of lumped pumps is inefficient. Therefore, a nonevaporable getter (NEG) is applied to the inner surface of the vacuum chamber. The getter is based, for example, on a Ti–Zr–V alloy. It efficiently absorbs the gases (except inert ones) and decreases the photodesorption from the chamber walls [74]. A differentially pumped vacuum has been actively used in individual components for a long time (for example, in small-aperture undulator chambers); however, MAX IV is the first accumulator in which the getter covers 100% of the vacuum chamber surface.

In magnetic blocks, the vacuum chamber is cylindrical and made of copper (to increase the thermal conductivity). In the median plane, it is connected via electron-beam welding with a water-cooled distributed radiation absorber, which effectively absorbs the SR heat with a power density up to 9.4 W mm^{-2} [75]. Some parts of the vacuum chamber (lumped pumping ports, chambers for fast dipole orbit correctors, and beam position sensors) are made of stainless steel. Straight sections contain special chambers (for injection, beam diagnosis devices, etc.), several ion pumps, and standard vacuum equipment (valves, bellows, residual gas pressure sensors, etc.)

The high-frequency accelerating system of MAX IV is quite conventional and includes six resonators at a frequency of 99.931 MHz, which provide the maximal accelerating voltage up to 1.8 MV. The advantages of using the low frequency (which is traditional for the MAX IV laboratory [76]) are the low voltage, sufficient for providing large energy acceptance, a long bunch, which reduces the resistive wall instabilities, and the existence of commercially available solid-state RF generators (FM range). Moreover, there are three passive resonators installed on the ring (the field in them is induced by the flight of the bunch), which operate at the third harmonic of the fundamental frequency and lengthen the beam by approximately a factor of five [77].

In order to reduce the influence of the coherent instabilities, it was decided to operate only in the multibunch regime, in which the intensity of each bunch is small. The low frequency of the RF system and third-harmonic resonators increase the threshold currents for coherent instability development.

Modern experiments with SR need the maximum stability of the beam orbit and current. For this reason, the top-up injection of new particles with the aim to compensate the losses corresponds to a beam lifetime of ≈ 10 h and is performed at the energy of 3 GeV. The particle source is a linear accelerator that operates at a 10 Hz repetition rate and 3 nC charge of each outgoing bunch ($\approx 0.3\%$ of the charge corresponding to the 500 mA accumulator current). The traditional injection scheme with the accumulated beam orbit bump towards the injected beam is typically realized using four kicker magnets, and it leads to large residual oscillations. Therefore, a new injection type was adapted using a nonlinear kicker magnet, in which the field is zero in the vicinity of the accumulated beam and is maximal in the vicinity of the injected beam [78].

The thoroughness of the project and the high fabrication quality of the systems and elements of the storage ring resulted in a quick and efficient start of the MAX IV SR source. The first beam was injected in August 2015, accumulation was achieved in September, and two undulators with a 7 mm gap were installed in February 2016. In May 2016, at the International Particle Accelerator Conference, the MAX IV representatives reported a circulating current ≈ 180 mA, the beam lifetime ≈ 10 h, and the measured emittance $\varepsilon_x = 300$ pm [79]. Figure 17 shows the general view of the MAX IV ring.

6.2 ESRF–EBS synchrotron radiation source

If MAX IV is the first circular SR source of the fourth generation, the ESRF–EBS device is a major upgrade of the ESRF third-generation SR source, which has been successfully operating in Grenoble since 1994. The difficulty is that the new storage ring, with a 30 times smaller emittance, had to be installed in the same tunnel. Moreover, because the construction of channels for SR output and experimental

Figure 17. MAX IV accumulator. A series of identical magnetic blocks can be seen. In the foreground, there is a small-aperture vacuum chamber of the straight section.

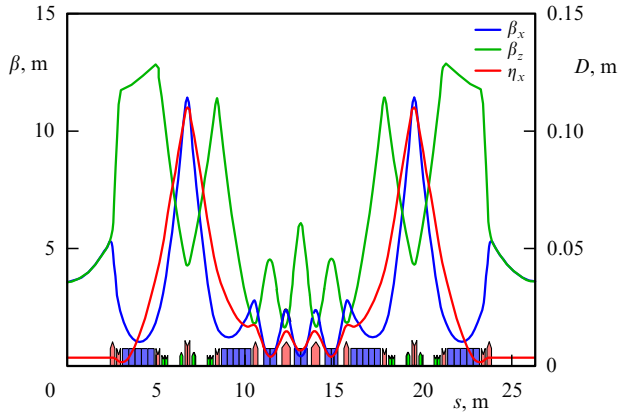

Figure 18. Optical functions of the ESRF–EBS superperiod.

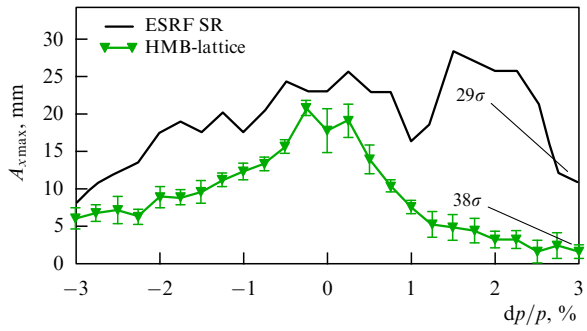

Figure 19. Horizontal dynamic aperture (for $\beta_x = 17$ m) versus the relative deviation of the particle momentum from the equilibrium value of the 'old' ESRF (ESRF–SR (synchrotron radiation)) and ESRF–EBS (HMB lattice) [80].

stations is a very complicated and expensive task, the upgrade must preserve all the 30 experimental lines made of straight sections. The new storage ring uses the old injector facility, with minor changes. Project development started in 2009 and its realization began in 2015.

ESRF–EBS consists of 30 standard superperiods and of two modified superperiods designed for the installation of injection devices and accelerating resonators. A hybrid multibend achromat lattice is used in the standard cells [80]. Its magnetic elements and lattice functions are shown in Fig. 18.

As we have mentioned, low emittance can be efficiently obtained by decreasing the magnet bending angle θ, because $\varepsilon_x \propto \theta^3$ [see (43)]. In this case, the dispersion function in the gaps is small, $\eta \propto \theta^2$, and the chromaticity correction requires strong sextupole lenses, which decrease the dynamic aperture. Therefore, the 7BA superperiod was modified by increasing the gaps between the first and the second magnets and between the sixth and the seventh magnets, such that the dispersion and betatron functions were significantly increased compared with those in the regular part (consisting of magnets 3–5). Initially, this cell was proposed for the project of an Italian Super B-factory electron–positron collider [81].

It can be seen from Fig. 18 that if the dispersion function value in the regular part of the cell is $\eta_{\max} \approx 1.5$ cm, then $\eta_{\max} \approx 12$ cm in the dispersion bump region. Large values of the betatron and dispersion functions, according to (68), allow using sextupoles with a relatively low gradient $B''_{\max} = 1500$ T m^{-2} (about 1/3 that in MAX IV) with a smaller number of lenses, which is favorable for the dynamic aperture. Moreover, the betatron phase increase between sextupole lenses at the beginning and at the end of the cell equals 3π for the horizontal lenses, and π for the vertical lenses, and hence in both cases the coordinate transformation between two identical sextupoles is described by minus the identity matrix. It is known that nonlinear aberrations of the sextupole lens system are suppressed in this case [82]. Like MAX IV, ESRF–EBS uses octupole magnets to control the betatron oscillation frequency dependence on the amplitude.

For the optimization of the dynamic structure (which is necessary for the effective injection) and dynamic energy acceptance (which is needed for a large Touschek lifetime), a nondominated sorting genetic algorithm II (NSGA II) was used [83]. These efforts resulted in absolute values of the dynamic aperture and acceptance that are only slightly lower than the ESRF ones (Fig. 19). Moreover, because the ESRF–EBS emittance is significantly lower than the ESRF emittance, in terms of the standard beam size, the aperture of the new SR source is even larger than that of the previous design.

The ESRF–EBS magnets are very diverse and complicated [84]. Three central bending magnets (3–5) have four poles (Fig. 20a) and are a combination of a weak dipole component with $B_{\max} = 0.57$ T and a quite large gradient $B'_{\max} = -37$ T m^{-1}. Four edge bending magnets of a superperiod (1, 2, 6, and 7) are fabricated based on the Sm_2Co_{17} permanent magnet technology from five sections with different fields in the range from 0.55 T to 0.16 T. Such dipoles with a step-like longitudinal field gradient (Fig. 20b) allow additional emittance reduction, as was described in Section 4.2.

Small-aperture quadrupole lenses (25 mm in diameter) provide a gradient up to 90 T m^{-1}. In sextupole lenses with a 38 mm aperture, the maximal sextupole gradient is $B''_{\max} = 1700$ T m^{-2}. The octupole lenses provide the maximal octupole gradient $B'''_{\max} = 36$ kT m^{-3} with an aperture of 37 mm. Moreover, there are lumped dipole orbit correctors, which compensate the winding in the sextupole lenses (dipole horizontal and vertical, as well as ones creating a skew quadrupole moment), low-current field correction windings in the magnets with longitudinal gradient, etc. The total number of ESRF–EBS magnets is over one thousand.

Sixteen ESRF experimental stations used hard X-ray radiation from bending magnets. Now, due to the increase in the number of bending magnets and decrease in the field amplitude, the SR spectrum becomes soft, and scientists are considering the possibility of installing short (with a bending

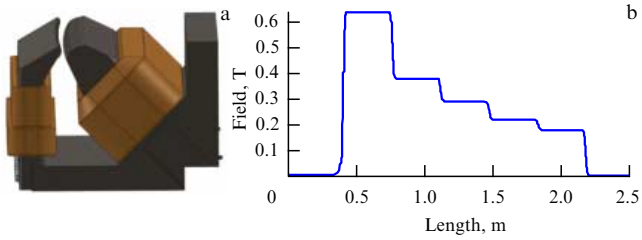

Figure 20. (a) Lower half of the ESRF–EBS dipole–quadrupole magnet. (b) Longitudinal distribution of the magnet field with a longitudinal gradient.

angle of several milliradians) high-field magnets with single and two- or three-pole wigglers.

The ESRF–EBS accelerating system works at the 352.2 MHz frequency [85]. Due to the decreased field of the magnets, the electron energy losses are reduced from 5.5 MeV to 3.3 MeV per revolution, which allows reducing the resonator voltage from 9 MV to 6 MV. Such a voltage provides energy acceptance at the level of $\pm 4.9\%$, which is enough to obtain a large Touschek lifetime. Twelve copper resonators with an accelerating-voltage higher-mode suppression system will be installed in two straight sections. The power of one RF generator is 100 kW for a beam current of 200 mA. As with MAX IV, the possibility of a third harmonic passive resonator installation is being considered. These resonators would lengthen the beam from 3 to 15 mm, increase the Touschek lifetime several-fold [86], and weaken the collective beam interaction with the chamber.

The main part of the vacuum chambers is fabricated from aluminum alloy using the extrusion method. Due to the low gas conductivity of narrow chambers, a nonevaporable getter coating is applied to the inner surface of the chambers, but lumped ion pumps are also actively used. The vacuum chamber is not cooled. Magnet radiation is captured by lumped copper absorbers of various types. The full SR power absorbed by the absorbers is more than 500 kW. The maximum power density of radiation on the absorbers is approximately 110 W mm^{-2}.

The beam is injected in ESRF–EBS with an energy of 6 GeV. For this, an existing injecting facility is used which includes a linear accelerator with an energy of 200 MeV and a booster synchrotron with an orbit length of 300 m and a 10 Hz repetition rate, which is slightly upgraded in order to decrease the emittance of the output beam. A new portion of electrons enters the ring using a traditional scheme with the horizontal offset in the same way as was done at ESRF. In this scheme, the accumulated beam is locally bumped by four kicker magnets towards the injected beam right before the injection moment in order to decrease the remaining oscillations. To increase the efficiency, the ESRF–EBS injection superperiod is modified: the horizontal betatron function at the injection azimuth is increased from $\beta_{x\mathrm{i}} \approx 6$ m to $\beta_{x\mathrm{i}} \approx 18-20$ m. This, together with a reduction in the injected beam emittance, results in an injection coefficient (corresponding to the results of many-particle simulations) up to $\approx 92-95\%$.

Much attention is paid to the decrease in the transition time from the old ESRF to ESRF–EBS. The superperiod in Fig. 18 is separated into four modules, each of which is assembled in advance and is installed on a precisely fabricated stage, which is then transported into the tunnel. Three months are given for the ESRF disassembly and eight months for the assembly of the new ring. The launch of the facility is planned to take only one month, and four more months will be needed for the reconstruction of the channels for the radiation output and experimental stations. The beginning of routine user work is scheduled for May–July 2020.

6.3 Storage ring projects with ultralow emittance

The examples considered above allow us to formulate the main features of new-generation storage rings with ultralow emittance:

- MBA magnetic lattice, compact superperiod, short magnets with a small bending angle;
- dipoles with combined functions (defocusing), a strong transverse gradient (up to approximately -40 T m^{-1}), dipoles with a longitudinal gradient;
- strong focusing and, as a consequence, large quadrupole lens gradients (up to ~ 100 T m^{-1}) with a small pole-to-pole diameter;
- Small dispersion function and strong sextupole lenses (up to $\sim 2-10$ kT m^{-2}), which compensate the natural chromaticity;
- high accuracy of fabrication and relative positioning of magnet elements ($\sim 10-20$ μm);
- small-aperture vacuum chamber (approximately 20–30 mm in diameter), intense use of differential pumping using NEG coatings;
- small dynamic aperture, which is increased by using octupole lenses, computer optimization of several sextupole lens families, application of complicated optical solutions (minus the identity transformation of the coordinates between sextupole pairs, local dispersion increase, etc.);
- additional reduction of the emittance using wigglers;
- strong betatron coupling (several percent), because for such a low horizontal emittance, the vertical one quickly reaches values comparable to the diffraction limit.

Many SR laboratories have announced the development of facilities similar to MAX IV and ESRF with the emittance < 1 nm. These are either new devices (similar to MAX IV), such as the Beijing Advanced Photon Source (BAPS) in China or Sirius in Brazil, or storage rings that use the existing infrastructure (like ESRF–EBS), including Diamond in Great Britain, SOLEIL in France, Spring-8 in Japan, and APS in the USA (see, e.g., [87] and the references therein). We note that new technologies allow 'transforming' not only the third-generation SR sources into the fourth-generation ones, but also the second-generation (a few remaining facilities) into third-generation ones. It is shown in [88] how the ANKA storage ring emittance can be reduced from the initial 90 nm to 9 nm; in [89], an upgrade of the Photon Factory (Japan) is described, resulting in a horizontal emittance reduction from 35 nm to 8 nm.

The most ambitious projects have a goal of obtaining the emittance significantly lower than 100 pm, reaching even diffraction limit (75). For a hard X-ray range, we assume $\lambda = 1$ Å and $\varepsilon_{x,y} \approx \varepsilon_{\mathrm{r}} = 8$ pm, and for a soft range, $\lambda = 10$ Å and $\varepsilon_{x,y} \approx \varepsilon_{\mathrm{r}} = 80$ pm [90]. These storage rings can be considered the 'generators' of ideas and approaches for the next breakthrough in relativistic electron beam emittance reduction. Table 5 provides examples of such projects. We note that although work on the project continues, the situation at the moment of publication can be different from the presented one.

All problems regarding the emittance reduction are also inherent in these rings, but more intensively (very strong sextupole lenses, the dynamic aperture around $\pm 1-2$ mm, a low threshold of microwave instability development, etc.). We consider two features. The very small dynamic aperture does not allow injecting the beam, which is shifted with respect to the accumulated one in the transverse phase volume. For this reason, other injection schemes are being investigated. Due to strong intra-beam scattering, the intensity of a single bunch is small (which is compensated by a large number of bunches) and the injector performance suffices to fully replace some of the bunches without accumulation. In this case, the bunch train is swapped out of the storage ring with short ($\sim 10-20$ ns) electromagnetic

Table 5. SR sources with ultralow emittance [90].

Project	E, GeV	Π, km	Lattice	ε_0, pm	σ_δ, %	Reference
USR7	7	3.16	10BA×40	30	0.079	[91]
PEP-X ultimate	4.5	2.2	7BA×48	24	0.13	[92]
Split-TME (IYsF)	3	2.43	7BA×45	10	0.025	[93]
IU ring	5	2.66	10BA×40	9.1	0.038	[94]
τUSR	9	6.21	7BA×180	2.9	0.096	[95]

pulses from a kicker, and a new portion is injected into the vacant position (so-called swap-out injection [96]). Another option is injection in the equilibrium orbit in the longitudinal phase space by using either a very fast kicker ($\sim 1-3$ ps) [97] or wo frequencies of the accelerating system (fundamental and doubled) [98]. In the latter case, the separatrix of the fundamental frequency is divided into two by the auxiliary frequency and a new bunch is injected into the newly formed vacant separatrix. After that, the auxiliary RF system is turned off and the injected bunch reaches equilibrium.

Another feature of diffraction-limited emittance storage rings is the expediency of having equal phase volumes: $\varepsilon_x = \varepsilon_y \approx \varepsilon_r$. In this case, the radiation brightness reaches its maximum, the optics for SR focusing on the sample is simplified, and intra-beam scattering is decreased (Fig. 21).

Round beams can be created using different methods, for example, by choosing the operating frequency point close to the coupling resonance and introducing skew quadrupoles or solenoids (realized for electron storage rings in [99]). Another way is to use wigglers with a horizontal field. In the framework of a project, an MBA lattice was developed in [100] with a relatively large horizontal emittance, $\varepsilon_{x0} = 80$ pm. After that, using superconducting multipole wigglers with a horizontal field of 4 T, the horizontal phase volume was decreased (due to an additional radiation reaction force) and the vertical one was increased (due to the appearance of quantum induced oscillations) in accordance with

$$\varepsilon_x = C_q \frac{\gamma^2}{J_x} \frac{I_{5x}}{I_{2x} + I_{2wy}} \approx C_q \frac{\gamma^2}{J_x} \frac{I_{5x}}{I_{2wy}} ,$$

$$\varepsilon_y = C_q \frac{\gamma^2}{J_y} \frac{I_{5wy}}{I_{2x} + I_{2wy}} \approx C_q \frac{\gamma^2}{J_y} \frac{I_{5wy}}{I_{2wy}} .$$

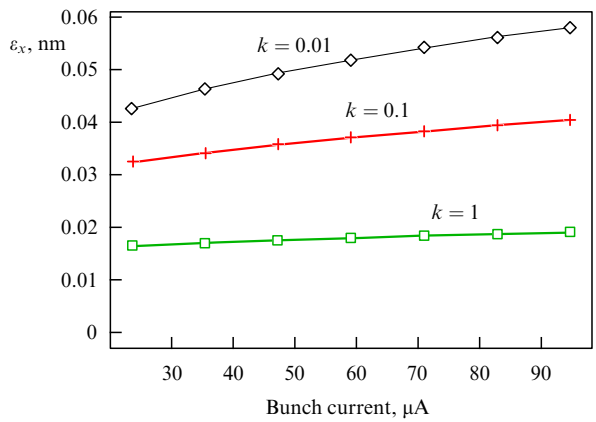

Figure 21. Emittance increase due to intra-beam scattering for different values of the betatron coupling constant.

The parameters were chosen such that for a beam current of 200 mA with intra-beam scattering taken into account, the emittance would be $\varepsilon_x = \varepsilon_y \approx 15$ pm.

7. Conclusions

We have discussed new physical and technological aspects related to electron storage rings with a small transverse phase volume. The author hopes that his work may be useful for the development of a modern SR source in Russia.

Acknowledgments
The study was supported by the Russian Science Foundation (project 14-50-00080). The author thanks N A Vinokurov and E A Perevedentsev for reading the manuscript and the helpful comments.

References

1. Emma P, Raubenhemier T *Phys. Rev. ST Accel. Beams* **4** 021001 (2001)
2. Raimondi P, Shatilov D N, Zobov M, physics/0702033; LNF-07/003 (IR) (2007); https://dx.doi.org/10.15161/oar.it/1449009600.96
3. Mobilio S, Boscherini F, Meneghini C (Eds) *Synchrotron Radiation: Basics, Methods and Applications* (New York: Springer, 2015)
4. Briggs R J et al., in *Proc. of the 1987 IEEE Particle Accelerator Conf., Accelerator Engineering and Technology, March 16–19, 1987, Washington, DC* Vol. 1 (Eds E R Lindstrom, L S Taylor) (Washington, DC: IEEE, 1987) p. 178
5. Kulipanov G N et al., in *ERL2011. Proc. of the of the 50th ICFA Advanced Beam Dynamics Workshop on Energy Recovery Linacs, KEK, Tsukuba, Japan, October 16–21, 2011* (Ed. A Shirakawa) (Tsukuba: KEK, 2011) p. 60
6. Willeke F, BNL-107934-2015-CP (New York: Brookhaven National Laboratory, 2015); https://www.bnl.gov/isd/documents/88771.pdf
7. Eriksson M et al., in *Proc. of the IPAC2011, 2nd Intern. Particle Accelerator Conf. 2011, San Sebastian, Spain, 4–9 September 2011* (San Sebastian: IPAC, EPS-AG, 2011) p. 3026
8. Revol J-L et al., in *IPAC2014. Proc. of the 5th Intern. Particle Accelerator Conf., June 15–20, 2014, Dresden, Germany* (Eds C Petit-Jean-Genaz et al.) (Dresden: IPAC, EPS, 2014) p. 209
9. Winick H *J. Synchr. Rad.* **5** 168 (1998)
10. Hettel R, in *IPAC2014. Proc. of the 5th Intern. Particle Accelerator Conf., June 15–20, 2014, Dresden, Germany* (Eds C Petit-Jean-Genaz et al.) (Dresden: IPAC, EPS, 2014) p. 7
11. Anashin V V et al. *Nucl. Instrum. Meth. Phys. Res. A* **282** 369 (1989)
12. Levichev E B *Phys. Part. Nucl. Lett.* **13** 876 (2016); *Pis'ma Fiz. Elem. Chast. At. Yad.* **13** 1365 (2016)
13. Courant E D, Snyder H S *Ann. Physics* **3** 1 (1958)
14. Jackson J D *Classical Electrodynamics* (New York: Wiley, 1999)
15. Wolski A, in *CAS — CERN Accelerator School: Advanced Accelerator Physics Course, Trondheim, Norway, 18–29 August 2013* (CERN-2014-009, Ed. W Herr) (Geneva: CERN, 2014) p. 245; https://dx.doi.org/10.5170/CERN-2014-009.245; arXiv:1507.02213
16. Helm R H et al. *IEEE Trans. Nucl. Sci.* **20** 900 (1973)
17. Bruk G *Tsiklicheskie Uskoriteli Zaryazhennykh Chastits* (Moscow: Atomizdat, 1970) original edition in French, see [60]

18. Robinson K W *Phys. Rev.* **111** 373 (1958)
19. Sands M "The physics of the electron storage rings. An introduction", in *Physics with Intersecting Storage Rings, Proc. of the Intern. School of Physics, Enrico Fermi, Course XLVI, 16 – 26 June 1969, Varenna, Italy* (Ed. B Touschek) (New York: Academic Press, 1971) p. 257; Report SLAC-121 (1970)
20. Chasman R, Green G K, Rowe E M *IEEE Trans. Nucl. Sci.* **22** 1765 (1975)
21. Korchuganov V N et al. *Nucl. Instrum. Meth. Phys. Res.* **208** 11 (1983)
22. Sommer M "Optimization of the emittance of electrons (positrons) storage rings", Report LAL-RT–83-15 (Orsay: Lab. de l'Accelerateur Lineaire, 1983)
23. Kamiya Y, Kihara M "On the design guideline for the low emittance synchrotron radiation source", Report KEK–83-16 (Oho, Ibaraki: National Lab. for High Energy Physics, 1983)
24. Leeman S C et al. *Phys. Rev. ST Accel. Beams* **12** 120701 (2009)
25. Lee S Y *Phys. Rev. E* **54** 1940 (1996)
26. Xu G, Peng Y-M *Chinese Phys. C* **39** 037005 (2015)
27. Helm R H, Wiedemann H, SLAC-PEP-Note–303 (1979)
28. Budker G I, Protopopov I Ya, Skrinskii A N, in *Trudy VII Mezhdunarodnoi Konf. po Uskoritelyam Zaryazhennykh Chastits Vysokikh Energii, Yerevan, 1969* Vol. 2 (Exec. Ed. A I Alikhanyan) (Erevan: Izd. AN ArmSSR, 1970) p. 37
29. Lightsource.org, http://www.lightsources.org/
30. Vignola G *Nucl. Instrum. Meth. Phys. Res. A* **246** 12 (1986)
31. Petrucci G, Tommasini D, in *Proc. of the 1993 Particle Accelerator Conference, PAC93, May 17 – 20, 1993, Washington, D.C., USA* (Eds S T Corneliussen, L Carlton) (Piscataway, NJ: IEEE, 1993) p. 2820
32. Keller R, in *Proc. of the 1993 Particle Accelerator Conference, PAC93, May 17 – 20, 1993, Washington, D.C., USA* (Eds S T Corneliussen, L Carlton) (Piscataway, NJ: IEEE, 1993) p. 2811
33. Kim D E et al., in *Proc. of the 23rd Particle Accelerator Conf., 4 – 8 May 2009, Vancouver, Canada* (Vancouver: PAC, 2010) p. 208
34. Nagaoka R, Wrulich A F *Nucl. Instrum. Meth. Phys. Res. A* **575** 292 (2007)
35. Guo J, Raubenheimer T, in *Proc. of the European Particle Accelerator Conf., EPAC 2002, Paris, France, 3 – 7 June 2002* (Paris: EPAC, 2002) p. 1136
36. Papaphilippou Y, Elleaume R, in *Proc. of the 2005 21st IEEE Particle Accelerator Conf., PAC 05, 16 – 20 May 2005, Knoxville, Tennessee, USA* (Ed. C Horak) (Piscataway, NJ: IEEE, 2005) p. 2086
37. Streun A, SLS Internal Report SLS-TME-TA-2006-0297 (Villigen: Paul Scherrer Institut, 2007); https://ados.web.psi.ch/slsnotes/tmeta060297.pdf
38. Wang C, Wang Y, Peng Y *Phys. Rev. ST Accel. Beams* **14** 034001 (2011)
39. Streun A "Longitudinal gradient super-bends and anti-bends for compact low emittance light source lattices", in *Low Emittance Rings Workshop IV, Frascati, September 17 – 19, 2014*, Presentation, slide 18
40. Papadopoulou S, in *Advanced Low Emittance Rings Technology, ALERT, Workshop, 5 – 6 May 2014, Valencia*
41. Baranov G, Levichev E, Sinyatkin S, arXiv:1504.01038
42. Baranov G, Levichev E, Sinyatkin S, in *Proc. of the 7th Intern. Particle Accelerator Conf., May 8 – 13, 2016, Busan, Korea* (Geneva: JACoW, 2016) p. 3014
43. Antokhin E I et al. *Nucl. Instrum. Meth. Phys. Res. A* **575** 1 (2007)
44. Vinokurov N A, Levichev E B *Phys. Usp.* **58** 850 (2015); *Usp. Fiz. Nauk* **185** 917 (2015)
45. Tischer M et al., in *Proc. of the 2005 21st IEEE Particle Accelerator Conf., PAC 05, 16 – 20 May 2005, Knoxville, Tennessee, USA* (Ed. C Horak) (Piscataway, NJ: IEEE, 2005) p. 2446
46. Baconnier Y et al. *Nucl. Instrum. Meth. Phys. Res. A* **234** 244 (1985)
47. Abaulrob H et al., in *IPAC'12. Proc. of the Intern. Particle Accelerator Conf., May 20 – 25, 2012, New Orleans, Louisiana, USA* (Piscataway, NJ, 2012) p. 702
48. Huang C W et al., in *IPAC2014. Proc. of the 5th Intern. Particle Accelerator Conf., June 15 – 20, 2014, Dresden, Germany* (Eds C Petit-Jean-Genaz et al.) (Dresden: IPAC, EPS, 2014) p. 2044
49. Goetsch T et al., in *IPAC2014. Proc. of the 5th Intern. Particle Accelerator Conf., June 15 – 20, 2014, Dresden, Germany* (Eds C Petit-Jean-Genaz et al.) (Dresden: IPAC, EPS, 2014) p. 2001
50. Cai Y Chou W (Ed.) *Beam Dynamics Newsletter* (57) (2012)
51. Chirikov B V "Issledovaniya po teorii nelineinogo rezonansa i stokhastichnosti", Preprint No. 278 (Novosibirsk: Institute of Nuclear Physics of the Siberian Branch of the USSR Academy of Sciences, 1969)
52. Laskar J *Astron. Astrophys.* **198** 341 (1988)
53. Bengtsson J *Beam Dynamics Newsletter* (57) 70 (2012)
54. Nadolski L S *Beam Dynamics Newsletter* (57) 85 (2012)
55. Streun A A *Beam Dynamics Newsletter* (57) 95 (2012)
56. Bartolini R *Beam Dynamics Newsletter* (57) 13 (2012)
57. Bernardini C *Phys. Persp.* **6** 156 (2004)
58. Bernardini C et al. *Phys. Rev. Lett.* **10** 407 (1963)
59. Touschek B, Report BNL-7534 (New York: Brookhaven National Laboratory, 1963)
60. Bruck H *Accélérateurs Circulaires de Particules* (Paris: Presses Univ. de France, 1966) translated into Russian, see [17]
61. Le Duff J, in *CAS — CERN Accelerator School: Accelerator Physics 14 – 25 Sep 1987, Berlin, Germany* (CERN 89-01, Ed. S Turner) (Geneva: CERN, 1989)
62. Piwinski A, in *Proc. of the 9th Intern. Conf. on High Energy Accelerators, Stanford, CA, May 2 – , 1974* (Stanford, CA: Stanford Linear Accelerator Center, Stanford Univ., 1974) p. 405
63. Bjorken J D, Mtingwa S K *Particle Accelerators* **13** 115 (1983)
64. Kubo K, Mtingwa S K, Wolski A *Phys. Rev. ST Accel. Beams* **8** 081001 (2005)
65. Bassetti M, Erskine G A "Closed expression for electrical field of a two-dimensional Gaussian charge", CERN-ISR-TH-80-06 (Geneva: CERN, 1980)
66. Venturini M, Oide K "Direct space charge effects on the ILC damping rings: Task Force Report", Report LBNL-59511 (Berkeley, CA: Lawrence Berkeley National Laboratory, 2006)
67. Boussard D "Observation of microwave longitudinal instablilities in the CPS", Report LABII/RF/Int./75-2 (Geneva: CERN, 1975)
68. Landau L D, Lifshitz E M *Electrodynamics of Continuous Media* (Oxford: Pergamon Press, 1984); Translated from Russian: *Elektrodinamika Sploshnykh Sred* (Moscow: Nauka, 1982)
69. Onuki H, Elleaume P (Ed.) *Undulators, Wigglers, and Their Applications* (London: Taylor and Francis, 2003)
70. Einfeld D et al., in *Proc. of the 1995 Particle Accelerator Conf. and Intern. Conf. on High-Energy Accelerators, May 1 – 5, 1995, Dallas, Texas* (Eds L T Gennari, R H Siemann) (Piscataway, NJ: IEEE, 1996)
71. Tavares P F et al. *J. Synchrotron Rad.* **21** 862 (2014)
72. Johansson M et al., in *Proc. of the IPAC2011, 2nd Intern. Particle Accelerator Conf. 2011, San Sebastian, Spain, 4 – 9 September 2011* (San Sebastian: IPAC, EPS-AG, 2011) p. 2427
73. Bjorklund Svenson J, Johansson M, in *Proc. of the 6th Intern. Particle Accelerator Conf., Richmond, VA, USA, May 3 – 8, 2015* (Geneva: JACoW, 2015) p. 57
74. Benvenuti C et al. *Vacuum* **53** 219 (1999)
75. Al-Dmour E et al. *J. Synchrotron Rad.* **21** 878 (2014)
76. Anderson A et al., in *Proc. of the 8th European Particle Accelerator Conf., EPAC2002, Paris, France, 3 – 7 June 2002* (Genava: EPAC, 2002) p. 2118
77. Skripka G et al., in *Proc. of the 7th Intern. Particle Accelerator Conf., May 8 – 13, 2016, Busan, Korea* (Geneva: JACoW, 2016) p. 2911
78. Atkinson T et al., in *Proc. of the IPAC2011, 2nd Intern. Particle Accelerator Conf. 2011, San Sebastian, Spain, 4 – 9 September 2011* (San Sebastian: IPAC, EPS-AG, 2011) p. 3394
79. Eriksson M et al., in *Proc. of the 7th Intern. Particle Accelerator Conf., May 8 – 13, 2016, Busan, Korea* (Geneva: JACoW, 2016) p. 11
80. Farvacque L et al., in *Proc. of the 4th Intern. Particle Accelerator Conf., IPAC2013, 12 – 17 May 2013, Shanghai, China* (Geneva: JACoW, 2013) p. 79
81. Biagini M E et al. "New low emittance lattice for the Super-B accelerator", Report SLAC-PUB-14652 (Stanford, CA: Stanford Linear Accelerator Center, Stanford Univ., 2011)
82. Brown K L *IEEE Trans. Nucl. Sci.* **26** 3490 (1979)
83. Deb K et al. *IEEE Trans. Evolut. Comput.* **6** 182 (2002)

84. Benabderahmane C et al., in *Proc. of the 7th Intern. Particle Accelerator Conf., May 8–13, 2016, Busan, Korea* (Geneva: JACoW, 2016) p. 1096
85. Serriere et al., in *Proc. of the IPAC2011, 2nd Intern. Particle Accelerator Conf. 2011, San Sebastian, Spain, 4–9 September 2011* (San Sebastian: IPAC, EPS-AG, 2011) p. 68
86. Carmignani N et al., in *Proc. of the 7th Intern. Particle Accelerator Conf., May 8–13, 2016, Busan, Korea* (Geneva: JACoW, 2016) p. 1644
87. Hettel R, in *IPAC2014. Proc. of the 5th Intern. Particle Accelerator Conf., June 15–20, 2014, Dresden, Germany* (Eds C Petit-Jean-Genaz et al.) (Dresden: IPAC, EPS, 2014) p. 7
88. Papash A et al., in *IPAC2014. Proc. of the 5th Intern. Particle Accelerator Conf., June 15–20, 2014, Dresden, Germany* (Eds C Petit-Jean-Genaz et al.) (Dresden: IPAC, EPS, 2014) p. 228
89. Harada K et al., in *Proc. of the 7th Intern. Particle Accelerator Conf., May 8–13, 2016, Busan, Korea* (Geneva: JACoW, 2016) p. 2874
90. Bei M et al. *Nucl. Instrum. Meth. Phys. Res. A* **622** 518 (2010)
91. Borland M *AIP Conf. Proc.* **1234** 911 (2010)
92. Nosochkov Y et al., in *Proc. of the IPAC2011, 2nd Intern. Particle Accelerator Conf. 2011, San Sebastian, Spain, 4–9 September 2011* (San Sebastian: IPAC, EPS-AG, 2011) p. 3068
93. Bogomyagkov A, Levichev E, Piminov P, arXiv:1405.7501; in *IPAC2014. Proc. of the 5th Intern. Particle Accelerator Conf., June 15–20, 2014, Dresden, Germany* (Eds C Petit-Jean-Genaz et al.) (Dresden: IPAC, EPS, 2014) p. 99
94. Cai Y *Nucl. Instrum. Meth. Phys. Res. A* **645** 168 (2011)
95. Jing Y, Ph.D. Thesis (Bloomington, IN: Indiana Univ., 2011)
96. Xiao A et al., in *25th North American Particle Accelerator Conf., NA-PAC'13, Pasadena, CA, USA, 29 September–4 October 2013* (Geneva: JACoW, 2013) p. 1076
97. Aiba M et al., in *IPAC2014. Proc. of the 5th Intern. Particle Accelerator Conf., June 15–20, 2014, Dresden, Germany* (Eds C Petit-Jean-Genaz et al.) (Dresden: IPAC, EPS, 2014) p. 1842
98. Jiang B C et al., in *Proc. of the 6th Intern. Particle Accelerator Conf., Richmond, VA, USA, May 3–8, 2015* (Geneva: JACoW, 2015) p. 1657
99. Danilov V V et al., in *Proc. of the Fifth European Particle Accelerator Conf., EPAC 96, Sitges, Barcelona, 10–14 June 1996* Vol. 2 (Ed. S Myers) (Boca Raton, FL: CRC Press, 1996) p. 1149
100. Bogomyagkov A V et al. "Proekt nakopitelya elektronov s emittansom, ogranichennym difraktsionnym predelom, i s bol'shoi dinamicheskoi aperturoi", Preprint No. 2013-28 (Novosibirsk: Institute of Nuclear Physics of the Siberian Branch of the Russian Academy of Sciences, 2013)